Available online at www.sciencedirect.com

ScienceDirect

Geochimica et Cosmochimica Acta 238 (2018) 208–234

Geochimica et Cosmochimica Acta

www.elsevier.com/locate/gca

Seasonal variations of biogeochemical matter export along the Langtang-Narayani river system in central Himalaya

Maya P. Bhatt [a,b,*], Jens Hartmann [a], Miguel F. Acevedo [b,c]

[a] Institute for Geology, Center for Earth System Research and Sustainability (CEN), Universität Hamburg, Bundesstrasse 55, D-20146 Hamburg, Germany

[b] Texas Environmental Observatory, University of North Texas, Denton, TX 76203-5017, USA

[c] Electrical Engineering Department and Advanced Environmental Research Institute, University of North Texas, Denton, TX 76203-5017, USA

Received 6 December 2016; accepted in revised form 28 June 2018; available online 7 July 2018

Abstract

Weathering and suspended matter fluxes of the Langtang Narayani river system in central Nepal Himalaya have been investigated at 16 stations for one year, based on monthly water sampling in the lower reaches and bi-monthly in higher elevation areas, to determine temporal variations of weathering fluxes along an elevation profile between 169 and 3989 m asl. Results indicate that the lower reaches are the dominant places of weathering in the system. The sum of major base cation fluxes is 2.9 to 9.2 higher during the monsoon season compared to the pre-monsoon season. Alkalinity and sea-salt corrected sulfate were the dominant anions (97%). The lowest downstream location exports 1611 tons km^{-2} yr^{-1} suspended sediment, 78.56 tons km^{-2} yr^{-1} of major cations (Na + K + Mg + Ca), 12.72 tons km^{-2} yr^{-1} of silica (4-fold higher than at the middle reaches of the basin), and 1.9×10^6 mol km^{-2} yr^{-1} of dissolved inorganic carbon (8.9-fold higher than at the middle reaches). Nitrogen and phosphorus concentrations are low in general and dissolved organic carbon export is within expected ranges. River water pCO_2 values are low in general, with exception of those main stem reaches where tributaries with relevant pyrite oxidation processes, and lower pH, alter the pattern locally. Element ratios suggest seasonal shifts in the weathering flux generation, modulated by the monsoon system. During the peak of the monsoon season the most relevant weathering products alkalinity, $^*SO_4$, $^*Ca$ and $^*Mg$ were not diluted, and increased concentrations observed at the lower reaches suggests an enhanced mobilization during this period of the year. Carbonate weathering exceeds silicate weathering along the drainage network and the carbonate- to silicate-cation mol ratio is 3.5 at the outlet. Sulfide oxidation probably enhances weathering rates besides the control of the soil-rock partial pressure of CO_2. The ratio of the total alkalinity flux to sea-salt corrected sulfate equivalent flux at the base of the Himalaya at Narayanghat was 5.7. Sea-salt corrected sulfate equivalent export is about the same as the silicate cation-equivalent flux that leaves the system (98%). Therefore, further research on sulfur isotopes might be helpful to support the hypothesis that pyrite oxidation compensates for the idealized CO_2-consumption by silicate weathering in the studied area.

Keywords: Weathering; Seasonality; Central Himalaya; Sulfide minerals; Elevation; Langtang – Narayani River

1. INTRODUCTION

Chemical weathering is an integral part of the rock and carbon cycle, resulting in dissolved ions and secondary minerals being transported by rivers to the ocean. Anderson et al. (2004) defined weathering as a complex suite of

* Corresponding author at: Texas Environmental Observatory, EE Department, Discovery Park, University of North Texas, Denton, TX 76203-5017, USA.

E-mail address: bhatt.maya@yahoo.com (M.P. Bhatt).

https://doi.org/10.1016/j.gca.2018.06.033

0016-7037/

chemical, biological, and physical processes. Long-term rapid uplift and erosion can be driven by plate tectonic processes, causing recycling of rocks within a basin and elevated denudation rates (Stallard, 2000).

There have been numerous studies in the field of geochemistry of river systems after the early works of Roth (1878, 1879, 1893) and Garrels and Mackenzie (1967, 1971), highlighting the relevance of weathering and land-ocean matter fluxes in the Earth system. Studies include those of the world's largest river systems resulting in flux baselines, variability, and identification of controls (Meybeck, 1982, 1987; Hu et al., 1982; Stallard and Edmond, 1983; Sarin et al., 1989; Degens et al., 1991; White and Blum, 1995; Gaillardet et al., 1999; Galy and France-Lanord, 1999; Singh et al., 2005; Hartmann et al., 2007). Moreover, global compilations of river chemistry data are now available (Hartmann et al., 2014).

Himalayan river systems have received much attention in recent decades due to the proposed connection between tectonic uplift in the region and global climate cooling caused by consuming atmospheric CO_2 through enhanced weathering rates (Raymo and Ruddiman, 1992; Edmond and Huh, 1997). However, recent studies suggest that chemical weathering in the Himalayan region itself represents a small fraction of weathering CO_2 consumption globally and thus may not have been able to contribute to global cooling in the Cenozoic (Galy and France-Lanord, 1999; France-Lanord et al., 2003; Wolff-Boenisch et al., 2009). Recent work on flood plain weathering below the Himalaya front suggests that the flood plains are a dominant location of silicate weathering of detrital material originating from the Himalaya (Lupker et al., 2012). Bickle et al. (2018) reported that chemical weathering fluxes in the flood plain area exceeds chemical weathering fluxes from the Himalayas.

Variation in chemical composition of river water along Himalayan river systems due to change in land use patterns and geomorphology have been observed and the role of runoff and physical erosion evaluated (France-Lanord et al., 2003; Singh et al., 2005; Bhatt et al., 2009). Gaillardet et al. (1999) estimated that 8.7×10^{12} mol yr^{-1} CO_2 are consumed globally by silicate weathering, while only 75 to 130×10^9 mol yr^{-1} CO_2 is consumed by silicate weathering in the Himalayan region of the Ganga basin. This latter estimate uses the value 0.4 to 0.7×10^6 mol km^{-2} yr^{-1} from Dalai et al. (2002) and a basin area of 187×10^3 km^2 from Galy and France-Lanord (1999). An estimated range of 0.2 to 0.3×10^6 mol km^{-2} yr^{-1} of consumed CO_2 by silicate weathering in Himalayan catchments (France-Lanord et al., 2003) is comparable to that of granitic basins (c.f. data in White and Blum, 1995; Oliva et al., 2003) but lower than that of basalt dominated basins in humid environments (Dessert et al., 2003; Börker et al., 2018). Similar CO_2 consumption rates by silicate weathering have been reported for the eastern Himalaya and Nepalese High Himalayan catchments (France-Lanord et al., 2003; Singh et al., 2005; Wolff-Boenisch et al., 2009).

Sulfide oxidation, often coupled with carbonate dissolution, influences the flux of dissolved inorganic carbon (DIC) in subglacial drainage systems within the Himalayan region and elsewhere (Tranter and Raiswell, 1991; Tranter et al., 1993; Galy and France-Lanord, 1999; Hasnain and Thayyen, 1999; Bhatt et al., 2000; Millot et al., 2003; Bhatt et al., 2009; Wolff-Boenisch et al., 2009; Bhatt et al., 2016; Torres et al., 2017). Sulphur oxidation may also be a relevant long-term source of CO_2 to the atmosphere-ocean system over long geological time scales (Torres et al., 2014).

Elements released along the central Himalayan river system result mainly from the dissolution of carbonate and silicate minerals (Galy and France-Lanord, 1999). Silicate weathering rates within the Himalayan landscape are also controlled by climatic related factors with considerable seasonality, such as runoff, as well as physical erosion (France-Lanord et al., 2003; West et al., 2005; Barnard et al., 2006; Tipper et al., 2006; Wolff-Boenisch et al., 2009). However, the monsoon effect on the chemistry of the waters draining a larger river basin from the glacial areas to the flood plains has not been studied using monthly sampling. The role of seasonality on the annual weathering fluxes across whole elevation transects in the Himalaya remains an open question.

For this purpose, we conducted this study along the Langtang – Narayani river system in central Nepal, to evaluate: (1) seasonal variations of surface water chemistry and fluxes of chemical species, (2) elevation variability of surface water chemistry in the context of factors that control chemical weathering rates, and (3) DIC fluxes and partial pressure of carbon dioxide (pCO_2) concentrations. This study uses data from monthly sampling at seven locations in the lower river reaches and bimonthly samples at nine locations in the high elevation areas along the Langtang-Narayani River. Importantly, the study was conducted before a major earthquake (7.8 magnitude) hit Nepal on April 25, 2015, causing at least 25,000 landslides throughout the central Himalayan Mountains in Nepal with more than half of the landslide volume directly connected to river channels (Roback et al., 2018). Therefore, results from our study offer a baseline prior to the reported landscape changes, including landslides and potential changes in hydrology. Future studies could then be used to examine to what extent earthquake activities are coupled to the long-term sediment budget and geochemical cycling in the Himalaya.

2. STUDY AREA

2.1. Site description

Located in the southern front of the Great Himalaya, the upper high Himalaya Langtang Lirung glacier (28°13′ 01.9″N, 85°33′42.0″E) is the headwater area of the Langtang-Narayani river system, reaching 7,234 m asl at its highest point. Ohata et al. (1987) reported that only 38.14% of the Langtang glacier head watershed (which is 333 km^2) was covered with glaciers at the time. The Trishuli basin is one of the major tributaries in the middle section of the Langtang-Narayani river system with a catchment area of 4,640 km^2. Downstream, the lower Narayani river at Narayanghat (27°41′58.1″ N, 84°25′17.6″ E) is in the

southern part of the Terai flood plain area in central Nepal (Fig. 1). In total, the Narayani river system has a basin area of 31,795 km^2. It is one of the major tributaries of the Ganga River, merging with it in India and ultimately entering the Bay of Bengal. Sampling was carried at different transects from the High Himalaya Langtang Lirung outlet point to the base of the Himalaya downstream at Narayanghat (Fig. 1 and Table 1).

Climate, terrain slope, soil, and vegetation vary widely along the Langtang-Narayani river system. Soil depth increases with decreasing elevation along the Langtang-Narayani river system. Vegetation ranges from sub-tropical forest, at low elevation area, to coniferous forest at higher elevations below the tree line, and negligible cover at high-altitude where the landscape consists of bare rock and talus with thin soils. At this high elevation, there is little

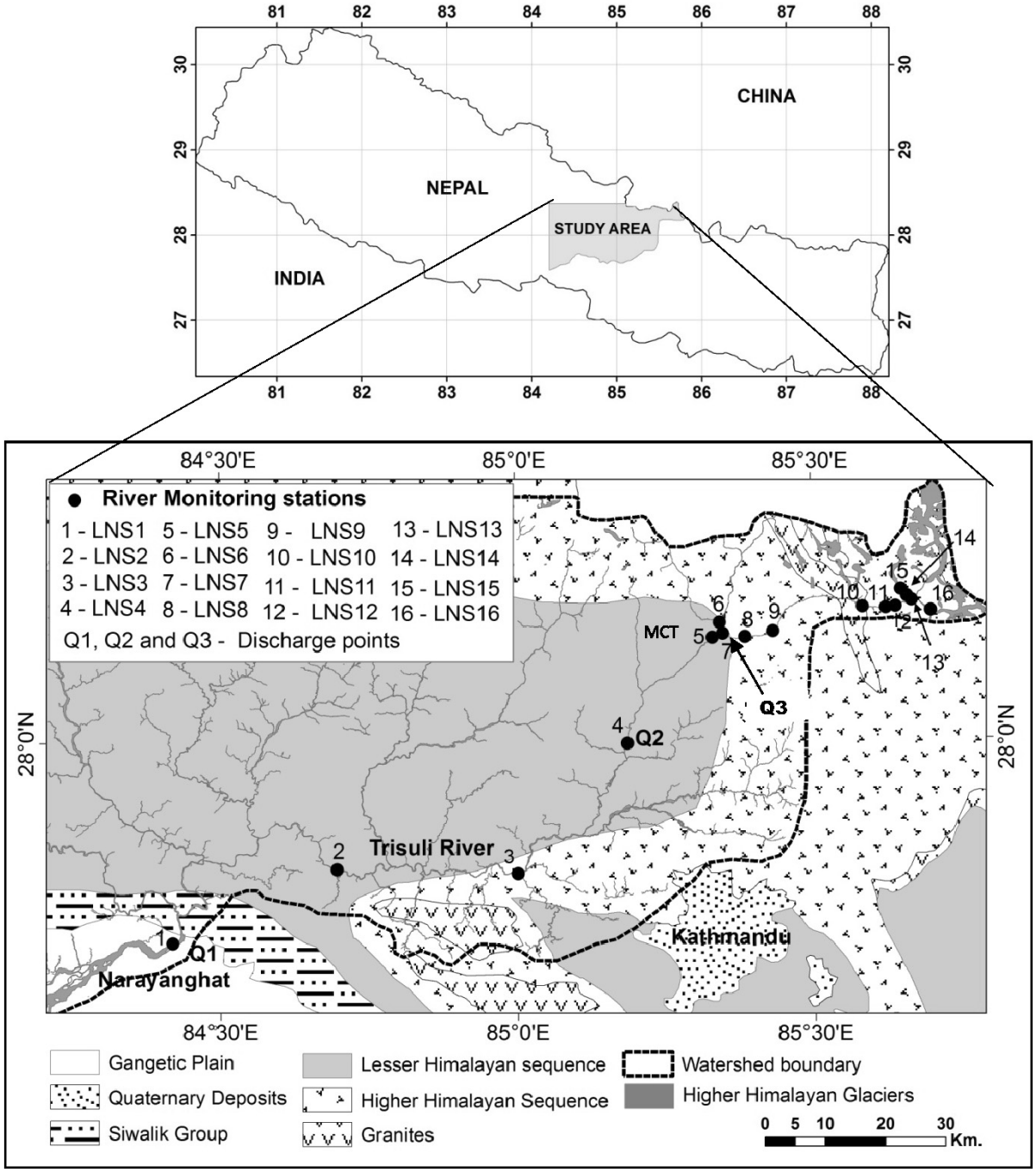

Fig. 1. Generalized geological map of Langtang Narayani river system in central Nepal with the sample locations represented by closed circles and labeled according to the inset. Table 1 provides longitude, latitude and elevation information. River discharge data was available for stations Q1 (LNS-1, Narayani river at Narayanghat), Q2 (LNS-4, Trishuli river at Betrawati), and Q3 (LNS-7, Langtang river at Syabrubensi), which are representative of low elevation, Siwaliks and Middle Mountain respectively.

Table 1
Sampling locations in the Langtang-Narayani River system.

Sample Name	River	Site	Drainage Basin**	Channel substrate	Vegetation type‡	Vegetation density	Latitude	Longitude	Elevation (m)
LNS-1	Narayani	Narayanghat	Terai	Clays and sand	Tropical forest	Dense	27°41′58.1″	84°25′17.6″	169
LNS-2	Trishuli	Fisling	Siwaliks	Sand, cobbles and boulders	Tropical forest	Sparse	27°50′39.3″	84°39′43.1″	258
LNS-3	Trishuli	Bairaini	Siwaliks	Sand and cobbles	Tropical forest	Sparse	27°48′03.9″	84°58′38.6″	377
LNS-4	Trishuli	Betrawati	Siwaliks	Sand, cobbles and boulders	Tropical forest	Dense	27°57′49.4″	84°10′24.9″	604
LNS-5	Langtang	Syabrubenshi	Midddle mountain	Cobbles and boulders	Sub tropical shrub	Sparse	28°09′52.3″	85°20′26.2″	1419
LNS-6	Bhotekoshi	Syabrubenshi	Midddle mountain	Cobbles and boulders	Sub tropical shrub	Sparse	28°09′56.9″	85°20′33.1″	1434
LNS-7	Langtang	Syabrubenshi	Midddle mountain	Cobbles and boulders	Sub tropical shrub	Sparse	28°09′47.9″	85°20′38.4″	1441
LNS-8	Langtang	Landslide	Midddle mountain	Cobbles and boulders	Sub tropical forest	Dense	28°09′05.9″	85°22′34.7″	1802
LNS-9	Langtang	Bamboo	Midddle mountain	Cobbles and boulders	Sub tropical forest	Dense	28°09′18.9″	85°23′52.0″	1864
LNS-10	Langtang	Ghodatabela	High Mountain	Sand, cobbles and boulders	Temperate forest	Dense	28°12′02.7″	85°27′44.5″	3034
LNS-11	Langtang	Kyangjin	High Mountain	Cobbles and boulders	Sub-alpine shrub	Sparse	28°12′34.6″	85°33′17.6″	3710
LNS-12	Lirung	Laja	High Mountain	Sand, cobbles and boulders	Sub-alpine shrub	Sparse	28°12′35.6″	85°33′22.5″	3703
LNS-13	Khimjung	Khimjung Khola	High Mountain	Clay, cobbles and boulders	Sub-alpine shrub	Sparse	28°12′58.1″	85°33′53.9″	3884
LNS-14	Lirung	Lirung Khola	High Mountain	Clay, cobbles and boulders	Sub-alpine shrub	Sparse	28°12′55.6″	85°33′49.9″	3882
LNS-15	Lirung	Lirung Outlet	High Mountain	Clay and boulders	Sub-alpine shrub	Negligible	28°13′01.9″	85°33′42.0″	3989
LNS-16	Langtang	Thumdi	High Mountain	Clay, cobbles and boulders	Sub-alpine shrub	Sparse	28°12′19.8″	85°34′04.1″	3800

‡ Stainton (1972) and Chaudhary et al. (2016).
** WWF Nepal (2005).

human influence due to seasonal settlement supported by subsistence farming and grazing by yaks and sheep. Agricultural activities may have partial impacts on water quality particularly by addition of nitrate, sulfate, and phosphate, occurring from the Middle Mountain areas to the lower Terai region.

2.2. Geologic setting

Geologically, the Himalayan basin is divided into four units from north to south separated by major thrust systems: the Tethyan Sedimentary Series (TSS), the High Himalaya Crystalline (HHC), the Lesser Himalaya (LH), and the Siwaliks (Gansser, 1964; France-Lanord et al., 2003). The headwater Langtang Lirung area lies in a complex transition zone between the HHC meta-sediments in the south and TSS in the north. Primarily, the Langtang watershed is underlain by high-grade metamorphic rocks with traces of igneous rocks, including migmatites, gneisses, schists, phyllites and granites (Inger and Harris, 1992). Based on X-ray fluorescence analysis of rock samples from the debris area of the Langtang Lirung Glacier (Bhatt et al., 2008), the bedrock consists of biotite, quartz, plagioclase with minor amount of muscovite, alkali feldspar, ilmenite and sillimanite. Biotite, quartz and plagioclase are the dominant silicates in the bedrock with lesser amounts of muscovite, alkali feldspar, ilmenite and sillimanite in the Himalayan region. In the high mountain region of central Nepal Himalaya, the major rocks are grey phyllites and grilstones with conglomerates and white massive quartzites, basic intrusion, grey calcareous slates and carbonates, as well as thick beds of grey siliceous dolomites (DMG, 1980, 1994). Cryothents, cryumbrepts, and lithic types of soils are dominant in the high elevation area of Langtang valley (SD, 1984).

The lesser Himalaya is composed of variable metamorphosed Precambrian sediments with quartzo-peltic schists, quartzites, and dolomitic carbonates (Gansser, 1964; Galy and France-Lanord, 1999). White massive fine to medium grained quartzites, green phyllites, basic intrusion, grey limestones and dolomites with thin intercalations of grey sales, white pink dolomitic limestones, purple quartzites and green shales are found in the middle mountain area (elevation range ~1,500–2,700 m asl) of central Nepal (DMG, 1980, 1994). Dominant soil types found in the central middle mountain region of Nepal include ustifluvents, eutrochepts, dystrochrepts, hoplumbrepts, lithic subgroups of eutrochepts and ustorthents, and ustorthents (SD, 1984).

In the southernmost part of the range, the geology consists of the recently uplifted Siwaliks, formed from Mio-Pliocene derail sediments accumulated in the previous Gangetic plain (Galy and France-Lanord, 1999; France-Lanord et al., 2003). Calcareous quartzites, limestones, black dark grey to greenish grey shales with intercalation of limestones and quartzites, coarse-grained sandstones, dark grey clays, silty sandstones to conglomerates are found in the low elevation Siwalik and Terai region of central Nepal (DMG, 1980, 1994). Dominant soil types in these low elevation areas are ustorthents, psamments, ustifluvents, fluvaquents, haplaquepts and halustolls (SD,

1984). The presence of sulfide bearing minerals such as pyrite, galena, sphalerite and pchalco pyrite enhance the dissolution rates of minerals within the basin (Bhatt et al., 2007).

2.3. Drainage basins by physiography

Nepal is divided into five physiographic divisions: Terai, Siwaliks, Middle Mountains, High Mountains, and High Himalayas (Kansakar et al., 2004; WWF Nepal, 2005). Elevation ranges for these five divisions are not very precise but we can approximately consider Terai being lower than 300 m, Siwaliks from 300 to 1,500 m, Middle Mountain from 1,500 to 2,700 m, High Mountain from 2,700 to 4,000 m, and the High Himalaya from 4,000 to 8,848 m. However, the Survey Department, SD (1983) considers Siwaliks from 300 to 700 m, Middle Mountain from 700 to 2,000 m, High Mountain 2,000 to 2,500 m, and High-Himalaya from 2,500 to 8,848 m. Due to wide variation in elevation with these physiographic divisions, there is wide variation in temperature, precipitation, runoff, physical erosion, vegetation and geology.

The High Himalaya region is home to eight of the world's highest mountains and the deepest gorge (5,791 m in the Kali Gandhaki) (WWF Nepal, 2005). Cool temperate climate and subalpine vegetation characterize the High Mountain region. Generally, soils in this region are young and thin, with a shallow regolith. In contrast, a deeper regolith occurs in the low elevation region where soils are older, thicker, more clayey, wetter and rich in organic matter.

Zonal movement of the summer monsoon, physiographic variation, and mountain relief exert control of precipitation patterns in Nepal (Kansakar et al., 2004). There was extensive deforestation in the lowland Terai and Siwalik regions in the past, and therefore landslides occur frequently in this region contributing large amounts of sediment transported through the river systems of these low elevation regions (WWF Nepal, 2005).

In addition to increased river discharge towards low elevation due to contribution from tributaries, precipitation varies widely along the drainage basin causing discharge variations at different transects of the basin (refer to Section 4.3). Furthermore, groundwater storage plays a major role in low elevation regions (Andermann et al., 2012). Seasonally, the highest discharge occurs during monsoon months (June to September), followed by the post-monsoon months (October to January) and least during the pre-monsoon months (February to May). In this work, we will follow this seasonal classification for the purpose of analysis.

3. MATERIALS AND METHODS

3.1. Sample collection

Surface water (including glacial melt water) sampling was carried out from the Lirung outlet point within the Langtang valley to Narayanghat at varying elevations (169–3,989 m asl) by selecting sixteen stations (LNS-1 to LNS-16) in this transect (Table 1). Water temperature (WT), electrical conductivity (EC) and pH were measured in the field by thermometer, EC meter (JENWAY EC-4200) and pH meter (TECPEL pH-873) respectively. The pH meter was calibrated every time before its use and after every five samples if the sample frequency was high. Water samples were analyzed for suspended sediments (SS), dissolved organic carbon (DOC), total dissolved nitrogen (TDN), dissolved silica (SiO_2), and major ions. Measurements and samples were taken from November 2010 to November 2011, except December 2010, on monthly basis or bimonthly basis depending on the variable measured and sampling station (Table 2).

Each water sample was filtered through a pre-combusted glass microfiber filter (Whatmann GF/F) with a pore size 0.45 μm for the DOC samples and polycarbonate microfiber filter with a pore size of 0.45 μm for the major ions and dissolved silica analysis. Samples were collected in 100 mL acid washed polyethylene bottles, kept refrigerated in Kathmandu, and sent with ice packs to the Institute for Biogeochemistry and Marine Chemistry of the Universität Hamburg (now Institute for Geology) for analysis. The DOC samples were taken in 30 mL glass vials in which 30 μl of phosphoric acid was added just after the filtration in the field. Pre-weighted filter papers were used to measure SS in each sample.

3.2. Analytical methods

The gravimetric method was used to measure SS on 47 mm GF/F and polycarbonate microfiber filter after drying in a vacuum oven at 40 °C for 48hr; the detection limit for SS was 1 mg L^{-1}. Alkalinity was estimated using a charge balance. Dissolved silica was analyzed with a DR 3800 spectrophotometer (HACH Company) using the standard molybdenum blue 8185 method.

Major cations Na^+, K^+, Mg^{2+}, Ca^{2+}, and NH_4^+, and major anions, F^-, Cl^-, NO_2^-, NO_3^-, and SO_4^{2-}, were determined by cation (Metrohm Compact IC pro 881-cation) and anion (Metrohm Compact IC pro 881-anion) chromatography, respectively. Anions were measured with a Metrohm self-regenerating suppressor MSM (50 mmol/L H_2SO_4) and analytical column Metrosep A SUPP 5-250 and cations with a Metrohm (C4) cation separation column (150 mm long). Analytical errors were <2% for Cl^-, NO_3^-, SO_4^{2-}, Na^+, K^+, Mg^{2+}, Ca^{2+}, and SiO_2, <4% for NH_4^+ and <5% for PO_4 – P. The precision was better than 5% and each sample was measured three times with reproducibility between 95 and 99%. We report SO_4^{2-} as sulfate measured directly by chromatography and not as sulfur.

High temperature Pt-catalyzed combustion, by Shimazdu TOC-V_{CSH} with a total-nitrogen measuring unit, was used to measure TDN and DOC. The dissolved inorganic carbon species including pCO_2 were calculated for a base elevation scenario for comparability using water temperature, pH, alkalinity, dissolved silica and major ions with the program PhreeqC V2 (Parkhurst and Appelo, 1999).

3.3. Silicate and carbonate weathering contributions

Chemical mass of the elements in a river system originates mainly from chemical weathering of minerals,

Table 2
Months sampled by station for groups of variables (x = WT and pH), (y = SS, SiO_2, and major ions), and (z = DOC and TDN). Also shown are total *n* of values available for analysis by month (nx, ny, and nz) and by station (mx, my, and mz). An x, y or z entry indicates that the variable of that group was sampled for that month and that station. EC is not shown and was sampled only on October 2011 from LNS-4 to LNS-16, and November 2011 from LNS-4 to LNS-7.

Station	2010		2011											nx	ny	nz
	Nov	Dec	Jan	Feb	Mar	Apr	May	Jun	Jul	Aug	Sep	Oct	Nov			
LNS-1	x,y,z		x,y		x,y,z	x,y,z	x,y,z	x,y,z	x,y,z	x,y,z	x,y,z	x,y,z	x,y,z	11	11	10
LNS-2	x,y,z		x,y		x,y,z	x,y,z	x,y,z	x,y,z	x,y,z	x,y,z	x,y,z	x,y,z	x,y,z	11	11	10
LNS-3	x,y,z		x,y		x,y,z	x,y,z	x,y,z	x,y,z	x,y,z	x,y,z	x,y,z	x,y,z	x,y,z	11	11	10
LNS-4	x,y,z		x,y,z	x,y,z	x,y,z	x,y,z	x,y,z	x,y,z	x,y,z	x,y,z	x,y,z	x,y,z	x,y,z	12	12	12
LNS-5	x,y,z		x,y,z	x,y,z	x,y,z	x,y,z	x,y,z	x,y,z	x,y,z	x,y,z	x,y,z	x,y,z	x,y,z	12	12	12
LNS-6	x,y		x,y	x,y,z	x,y,z	x,y,z	x,y,z	x,y,z	x,y,z	x,y,z	x,y,z	x,y,z	x,y,z	12	12	10
LNS-7	x,y		x,y	x,y,z	x,y,z	x,y,z	x,y,z	x,y,z	x,y,z	x,y,z	x,y,z	x,y,z	x,y,z	12	12	10
LNS-8	x,y,z		y,z		y,z		y,z		y,z		y,z	y,z		2	7	7
LNS-9	x,y,z		y,z		y,z		y,z		y,z		y,z	y,z		2	7	7
LNS-10	x,y,z		y,z		y,z		y,z		y,z		y,z	y,z		2	7	7
LNS-11	x,y,z		y,z		y,z		y,z		y,z		y,z	y,z		2	7	7
LNS-12	x,y,z		y,z		y,z		y,z		y,z		y,z	y,z		2	7	7
LNS-13	x,y,z		y,z		y,z		y,z		y,z		y,z	y,z		2	7	7
LNS-14	x,y,z		y,z		y,z		y,z		y,z		y,z	y,z		2	7	7
LNS-15	x,y,z		y		y,z		y,z		y,z		y,z	y,z		2	7	6
LNS-16	x,y,z		y		y,z		y,z		y,z		y,z	y,z		2	7	6
mx	16	0	7	4	7	7	7	7	7	7	7	16	7	99		
my	16	0	16	4	16	7	16	7	16	7	16	16	7		144	
mz	14	0	9	4	16	7	16	7	16	7	16	16	7			135

atmospheric input or cyclic salt, and anthropogenic input. The contribution of silicate and carbonate weathering was estimated based on the approach of Galy and France-Lanord (1999). For these relatively pristine Himalayan river systems, we considered anthropogenic sources as negligible and thus the concentration of an element [X] is estimated as

$$[X] = [X]_c + [X]_w \quad (1)$$

where the subscripts *c* and *w* stand for cyclic and weathering contributions respectively.

Sea-salt inputs to surface waters are estimated using molar ratios of elements found in seawater (Keene et al., 1986; McDowell et al., 1990; Millot et al., 2002; Bhatt and McDowell, 2007). River-water chloride concentration was used as a reference species to correct the contribution of sea-salt in surface waters for Na, K, Mg, Ca and SO_4. We subtracted sea-salt concentration from total measured concentration of the concerned element, using chloride-normalized ratios 0.8621, 0.0188, 0.1958, 0.0378, and 0.1043 for sodium, potassium, magnesium, calcium and sulfate, respectively (Keene et al., 1986). The sea-salt corrected concentration of each chemical species is represented with an asterisk

$$^*[X] = [X] - [X]_c = [X]_w \quad (2)$$

Input of major base cations due to chemical weathering comes primarily from weathering of carbonates and silicates within the Himalayan basin. Thus, after cyclic salt correction, the contribution of major base cations is

$$^*[X] = {}^*[X]_{car} + {}^*[X]_{sil} \quad (3)$$

where the subscripts *car* and *sil* stand for carbonate and silicate weathering respectively. We assume that the contribution of sodium and potassium after cyclic salt correction is from silicate dissolutions only as there is no contribution of these elements from carbonate dissolution. The contribution of evaporites to sodium weathering fluxes is assumed negligible for this basin. Thus, we can write

$$^*[Na]_{sil} \simeq {}^*[Na] \text{ and } {}^*[K]_{sil} \simeq {}^*[K] \quad (4)$$

Galy and France Lanord (1999) estimated the magnesium contribution from silicate weathering by multiplying the ratio of magnesium to potassium (0.5 ± 0.25) with the cyclic salt-corrected potassium concentration. Our concentration data show a high variability with a skewed distribution because of the influence of seasonality. At three sites, LNS-1, LNS-4, and LNS-7 we had data on water flow (see Section 3.5 below) allowing us to calculate flux. These stations are denoted Q1, Q2, and Q3 respectively. For all three sites with discharge measurements, the contribution of Mg to the total silicate weathering fluxes ($^*Sbcat_{sil}$) is relatively low (at LNS-1, the lowest monitoring location where the contribution is highest has a median of 15.5% and 95%-percentile of 25.6%). Whereas the Na plus K contribution to total silicate weathering ($^*Sbcat_{sil}$) is much higher (at LNS-1 the median contribution is 75.6%, and the 95% percentile 79.3%). The first quartile, median, and third quartile Mg concentration at Narayanghat (LNS-1, Q1) originating from silicate weathering is 29.0, 38.5 and 57.0 (in $\mu mol\ L^{-1}$), at Betrawati (LNS-4, Q2) 16.5, 25.0 and 32.8, and at Syabrubenshi (LNS-7, Q3) 14.6, 18.3 and 23.1, respectively.

We also observe a few *[Mg] to *[K] ratio values greater than 1. For catchments underlain by pure silicate rocks in the region the *[Mg] to *[K] ratios appears to be low, ranging from 0.2 to 1 (Galy and France-Lanord, 1999). Thus, we used the *[Mg] to *[K] ratios of 0.5 ± 0.25 as a first estimate:

$$^{*}[Mg]_{sil} \cong {}^{*}[K]_{sil} \times (0.5 \pm 0.25) \simeq {}^{*}[K] \times (0.5 \pm 0.25) \quad (5)$$

Total calcium concentration after cyclic salt correction from silicate weathering can be estimated by multiplying molar ratios of calcium to sodium ($Ca/Na = 0.2 \pm 0.02$) by the sea-salt corrected sodium (Galy and France Lanord, 1999). For all three sites with discharge measurements (where we can calculate flux), the calcium contribution to total silicate weathering ($^{*}Sbcat_{sil}$) is low (median 8.93% and 95%-percentile 12.6%, at LNS-1). The first quartile, median, and third quartile of Ca contribution to silicate weathering (in μmol L^{-1}) is 12.5, 17.6, 69.2 at Narayanghat (LNS-1, Q1), 10.7, 17.6, 41.6 at Betrawati (LNS4, Q2), and 6.75, 10.8, 42.0 at Syabrubenshi (LNS7, Q3), respectively.

The geology of our study area is similar to the study area of Galy and France-Lanord (1999) and the Ca/Na average ratios of whole silicate rock composition of eroded formations within the High Himalaya region is in the range of 0.18 to 0.25 (Brouand, 1989 as cited in France-Lanord and Derry, 1997; Galy and France-Lanord, 1999). Therefore, we use

$$^{*}[Ca]_{sil} \simeq {}^{*}[Na]_{sil} \times (0.2 \pm 0.02) \simeq {}^{*}[Na] \times (0.2 \pm 0.02) \quad (6)$$

Now, the total silicate contribution is the sum of base cations ($^{*}Sbcat_{sil}$) from silicate weathering only

$$^{*}Sbcat_{sil} = {}^{*}[Na]_{sil} + {}^{*}[K]_{sil} + {}^{*}[Mg]_{sil} + {}^{*}[Ca]_{sil} \quad (7)$$

Magnesium and calcium contributions from carbonate weathering can be estimated by subtracting silicate-weathering magnesium and calcium from total cyclic salt corrected magnesium and calcium respectively, therefore

$$^{*}[Mg]_{car} = {}^{*}[Mg] - {}^{*}[Mg]_{sil} \simeq {}^{*}[Mg] - {}^{*}[K] \times (0.5 \pm 0.25) \quad (8)$$

$$^{*}[Ca]_{car} = {}^{*}[Ca] - {}^{*}[Ca]_{sil} \simeq {}^{*}[Ca] - {}^{*}[Na] \times (0.2 \pm 0.02) \quad (9)$$

Total carbonate contribution is the sum of base cations from carbonate weathering only, which, using Eqs. (8) and (9), can be rewritten as

$$^{*}Sbcat_{car} \simeq {}^{*}[Mg]_{car} + {}^{*}[Ca]_{car} \quad (10)$$

In summary, we use Eqs. (7) and (10) to estimate the silicate and carbonate weathering contribution to the dissolved chemical species in the river water. To assess the propagation error due to the variability in the ratios $Ca/Na = 0.2 \pm 0.02$ and $Mg/K = 0.5 \pm 0.25$, we applied Monte Carlo resampling (Acevedo, 2013) by generating 1000 random samples of these ratios and calculating $^{*}Sbcat_{sil}$ and $^{*}Sbcat_{car}$ for each random sample. This allowed estimating the standard error of these values and their influence on subsequent calculations.

To be consistent with the literature, the concentration units were changed first into meq L^{-1} when correcting for cyclic salt inputs. Later we changed into molar units to make them comparable to silicate and carbonate contribution to total weathering. Finally, we estimated the contribution of each element in mol L^{-1} or mg L^{-1} as commonly reported in the literature.

3.4. Spatial and temporal variability

All measured physical and chemical variables were grouped by season (pre-monsoon, monsoon, post-monsoon). Their seasonal average and variability were then plotted as a function of elevation of the sixteen sampling stations (LNS-1 to LNS-16) to examine spatial variability. In order to study the temporal variability, we constructed complete time series for all measured water chemistry variables for the period November 2010 to November 2011. Because December 2010 was not sampled, the missing data were interpolated.

3.5. Hydrologic data and flux calculations

We examined river discharge data provided by the Department of Hydrology and Meteorology (DHM, 2008), Government of Nepal. As mentioned in Section 3.3, we used daily flow data from three locations (denoted here as Q1, Q2, and Q3) that corresponded to water chemistry stations LNS-1, LNS-4, and LNS-7 respectively. Of these, the highest location, Q3, is the Langtang River at Syabrubenshi, Middle Mountain (available data for 2010–2013). At intermediate altitude, the Q2 location is the Trishuli river at Betrawati (available data for 1983–2014), in the Siwaliks, and lastly at the base of the Himalaya, lower Terai plain, the location, Q1, is the Narayani river at Narayanghat (available data for 1963–2011) (Fig. 1).

Flow data from November 2010 to November 2011 was selected in order to correspond to our water-sampling period. Flow in $m^3 s^{-1}$ was normalized per unit of basin area (in km^2) and accumulated per year, to represent it as specific discharge or runoff q in m yr^{-1}. The catchment area of each station is 31,795 km^2 for Q1, 4,640 km^2 for Q2 and 583 km^2 for Q3.

For these three sampling stations, we examined concentration vs discharge plots using q in log scale as the horizontal axis variable. For each watershed and solute, we estimated the solute production using the model of Maher and Chamberlain (2014) as discussed in Ibarra et al. (2016)

$$C = C_{\max} \frac{D_w/q}{1 + D_w/q} = C_{\max} \frac{D_w}{q + D_w} \quad (11)$$

where C is the solute concentration in μmol L^{-1} (measured), C_{max} corresponds to the thermodynamic limit, estimated here to be the maximum concentration of a solute for each catchment, and D_w is the Damköhler coefficient in myr^{-1} (same units as runoff), which was estimated by non-linear regression using C and q data (Supplementary information Tables S1, S3, S4 and S5). For this purpose, we employed the nls-function of the program R (Acevedo, 2013; CRAN, 2018). We wrote a function that

finds the maximum value for each constituent, assigned this maximum to C_{max}, calculated a first estimate for D_w as the value of q for which the concentration attains $C_{max}/2$, then used this first estimate as argument in the function nls. This function successively iterates the estimate to determine the value of the parameter value D_w that produces the best fit by optimization.

In addition, we calculated area-normalized fluxes as the product of concentration (in mg L^{-1} for SS, DOC, TDN, and SiO_2 and mol L^{-1} for ions) and runoff in m yr^{-1}. Thus, the area-normalized flux was expressed in t km^{-2} yr^{-1} for SS, DOC, TDN, and SiO_2 and mol km^{-2} yr^{-1} for ions. For brevity, hereafter we will simply use the term flux to refer to the area-normalized flux.

To calculate the total annual export, we used the annual average of the product daily water flow times the corresponding concentration values (interpolated in a few cases of missing data). The total cationic flux was calculated from the Sbcat flux, which is the sum of major cations concentrations before sea-salt correction. Then its annual value was denoted as cation export rate. These annual cation and silica loads were then compared with other world rivers.

We included flux calculations for silicate and carbonate weathering contributions $^{*}Sbcat_{sil}$ and $^{*}Sbcat_{car}$. The cationic weathering flux after sea-salt correction was calculated as the flux of the sum of both $^{*}Sbcat = {}^{*}Sbcat_{sil} + {}^{*}Sbcat_{car}$ and then converted to annual cation denudation rate (CDR).

Finally, we use CDR to calculate $W^{\beta}{}_{D}$ or also known as "weathering advance rate of any scale" (Navarre-Sitchler and Brantley, 2007) using the equation

$$W^{\beta}{}_{D} = \frac{CDR}{\rho_p \alpha (1-\phi)} \tag{12}$$

where $W^{\beta}{}_{D}$ is given in mm^3 mm^{-2} kyr^{-1}, CDR in tons km^{-2} yr^{-1}, ρ_p is the density of parent rocks (g/cm^3), α is the ratio of base cations per g of parent rock, and ϕ is porosity of parent material. The Langtang-Narayani river system is mostly underlain by metamorphic terrane so we used the average rock density (2.78 g/cm^3) for metamorphic terrane range from 2.7 to 2.86 g/cm^3 (Smithson, 1971), and $\alpha = 0.15$ and $\phi = 0.1$ as a first estimate for the region.

4. RESULTS

Water quality variables, SS, DOC, TDN, SiO_2 and major ions, were measured for most months over the study period for stations LNS-1 through LNS-7, but only bimonthly for the higher elevation sampling locations LNS-8 through LNS-16 (Table 2, Table 3). Concentrations of ammonium and phosphate were often below detection limit or negligible and were therefore excluded from further analysis.

The major cation and anion compositions followed in general the order $Ca^{2+} \gg Mg^{2+} > Na^{+} \gg K^{+}$ and Alkalinity $\gg SO_4^{2-} \gg Cl^{-} > F^{-} > NO_3^{-}$ along the entire Langtang-Narayani drainage network. The sea-salt corrected $^{*}Na$, $^{*}K$, $^{*}Mg$, $^{*}Ca$, and $^{*}SO_4$, represent in this analysis the contribution from rock weathering, and were on average 80.3%, 99.1%, 96.8%, 99.9%, and 98.5% of the total

Table 3
Annual average of concentrations of major constituents along the Langtang Narayani river system in central Nepal. The standard deviations were calculated using n as given in Table 2. The full data set is provided in a Supplement Excel Table.

Sample Name	SS mg/L	DOC µmol/L	TDN µmol/L	Alkalinity µmol/L	F µmol/L	Cl µmol/L	SO_4 µmol/L	NO_3 µmol/L	Na µmol/L	K µmol/L	Mg µmol/L	Ca µmol/L	Si µmol/L
LNS-1	449 ± 586	139 ± 64	93 ± 82	2,316 ± 917	5.0 ± 1.1	142 ± 129	218 ± 71	52 ± 81	304 ± 260	100 ± 67	396 ± 156	877 ± 351	152 ± 40
LNS-2	488 ± 849	150 ± 59	58 ± 55	1,422 ± 412	6.4 ± 1.4	28 ± 16	189 ± 64	5.5 ± 7.7	152 ± 111	55.5 ± 18	210 ± 65	606 ± 168	121 ± 26
LNS-3	536 ± 867	129 ± 91	38 ± 27	1,143 ± 388	6.7 ± 1.5	32 ± 19	110 ± 37	5.4 ± 7.3	160 ± 113	66 ± 42	125 ± 41.1	466 ± 141	136 ± 26
LNS-4	210 ± 352	173 ± 45	51 ± 75	1,070 ± 442	13.4 ± 26.4	25 ± 19	106 ± 60	3.2 ± 2.6	153 ± 102	116 ± 212	124 ± 54	417 ± 191	125 ± 49
LNS-5	188 ± 282	150 ± 96	35 ± 39	1,016 ± 1,851	7.8 ± 2.1	30 ± 24	172 ± 80	5.5 ± 5.9	167 ± 143	44 ± 17	143 ± 81	494 ± 215	94 ± 27
LNS-6	167 ± 250	116 ± 79	23 ± 12	1,418 ± 521	8.2 ± 2.0	45 ± 27	201 ± 73	6.4 ± 6.6	196 ± 140	64 ± 49	173 ± 67	637 ± 213	98 ± 23
LNS-7	299 ± 601	108 ± 58	19 ± 8	642 ± 219	8.9 ± 2.1	18 ± 16	85 ± 27	5.2 ± 4.2	125 ± 95	40 ± 41	42 ± 22	295 ± 84	93 ± 23
LNS-8	240 ± 457	111 ± 37	16 ± 8	909 ± 890	9.6 ± 2.3	11 ± 6	80 ± 18	3.7 ± 4.1	120 ± 99	39 ± 16	36 ± 9	430 ± 419	89 ± 19
LNS-9	254 ± 563	146 ± 126	15 ± 9	659 ± 280	14.3 ± 12.6	13 ± 6	81 ± 17	2.7 ± 3.2	120 ± 100	48 ± 18	37 ± 10	304 ± 106	78 ± 21
LNS-10	100 ± 165	427 ± 453	27 ± 13	744 ± 405	10.3 ± 4.0	15.5 ± 8	92 ± 20	4.9 ± 5.2	130 ± 100	43 ± 17	47 ± 26	345 ± 158	81 ± 31
LNS-11	129 ± 194	144 ± 108	15 ± 7	704 ± 312	12.2 ± 3.5	10.6 ± 8	96 ± 25	4.2 ± 6.0	113 ± 100	38 ± 11	44 ± 10	343 ± 124	66 ± 25
LNS-12	40 ± 48	152 ± 90	20 ± 8	538 ± 386	8.1 ± 5.0	9.2 ± 7.6	82 ± 39	5.1 ± 5.8	95 ± 97	33 ± 15	36 ± 18	263 ± 167	57 ± 25
LNS-13	76 ± 54	121 ± 62	28 ± 26	605 ± 474	7.4 ± 4.9	7.3 ± 2.8	71 ± 43	4.6 ± 6.1	75 ± 76	31 ± 13	51 ± 42	278 ± 202	44 ± 20
LNS-14	88 ± 46	106 ± 59	31 ± 9	396 ± 255	6.2 ± 1.8	26.4 ± 50	105 ± 49	7.3 ± 8.0	84 ± 77	54 ± 52	26 ± 13	228 ± 127	43 ± 11
LNS-15	55 ± 34	138 ± 60	33 ± 11	396 ± 253	6.2 ± 1.8	7.9 ± 4.7	105 ± 48	7.0 ± 9.2	83 ± 75	37 ± 15	24 ± 11	229 ± 127	40 ± 9
LNS-16	109 ± 131	122 ± 58	23 ± 10	758 ± 375	15.3 ± 3.7	13.3 ± 10.6	101 ± 30	3.2 ± 4.3	127 ± 109	39 ± 15	45 ± 12	367 ± 151	69 ± 20

concentrations, respectively. In addition, the contribution of marine aerosols varied little with elevation, except for sodium (Table S2).

After sea-salt correction, the sum of divalent ions (calcium and magnesium) accounts for 85% of the total sum of all major cations, on average, whereas the sum of monovalent ions (sodium and potassium) contributes 15% to the total sum of the major cations (Table S2). Alkalinity contributes nearly 75% to the total sum of anions, and sulfate contributes 22% to the total sum of anions, on average (Table 3). Thus, sulfate and alkalinity account for most (~97%) of the total sum of anions. The contribution of fluoride (0.96%) and chloride (2.10%) to the total sum of anions was minor and accounts for most of the remainder, since that of nitrate contributed on average 0.47%.

Bicarbonate (HCO_3) is the dominant inorganic carbon species, contributing 85% to the total DIC followed by dissolved carbon dioxide (CO_2/H_2CO_3) and carbonate (CO_3) in the surface water. The river water was supersaturated with carbon dioxide (pCO_2) in Terai, Siwalik and the lower middle mountains region (LNS-1 through LNS-7) around the pre-monsoon period (February to May), elsewhere, a mixed picture is observed, with partly under-saturated conditions at sites LNS-8 through LNS-16 (Table S1), probably because sea level air pressure was assumed for the calculation. Results suggest that excess-CO_2 degassed rapidly in the steeper parts of the catchment, as river water in general supersaturated with respect to CO_2 (Kempe, 1982; Raymond et al., 2013; Lauerwald et al., 2015). Notable are relatively high pCO_2 values around stations LNS-5 to LNS-7, which correlate with a low pH (Table S1), which on average affects the calculation towards an overestimation (Abril et al., 2015). Therefore, the interpretation will be conducted qualitatively.

4.1. Spatial variability: elevational gradients by season

In the post-monsoon season, water temperature shows a clear decreasing trend with increasing elevation from the base of the Himalaya to the higher elevation sites in the high Himalaya within the Langtang valley (Figure S1a). The pH was in general between ~7 to 8 during the post-monsoon and the monsoon season, indicating that the surface water is slightly alkaline along the entire Langtang Narayani river system during those seasons. However, the water became slightly acidic during the pre-monsoon season below station LNS-7 (Figure S1b). EC ranged from 116 $\mu S\ cm^{-1}$ to 667 $\mu S\ cm^{-1}$ along the Langtang Narayani river system (graph not shown because it was measured only during fall).

SS concentrations show a decreasing trend with increasing elevation during the monsoon season (Figure S1c), which is in contrast with the pre-monsoon and the post-monsoon season with in general low concentrations. DOC concentrations did not show any clear trend with elevation if data for each season are considered. At higher elevations, pre- and post-monsoon season values are higher than during monsoon time. DOC fluctuates typically between 1 and 3 $mg\ L^{-1}$ for almost all sites except site (LNS-10) which had 2 to 5 times that value during the pre- and post-monsoon season (Figure S1d). Seasonality of TDN shows no clear trend with elevation, but higher values during the post-monsoon period in the lower reaches (Figure S1e). Dissolved Si shows a strong relationship with elevation along the entire river system for all seasons, with elevated concentrations in the higher areas during the non-monsoon time compared to the monsoon season, but with a mixed seasonal picture in the lower parts of the basin (Figure S1f).

The sum of anions shows an increasing concentration trend with decreasing elevation, with partly less pronounced trends, or no clear trend, for single anion species and different seasons (Fig. 2). Alkalinity shows a clear increasing trend towards lower sites for all seasons with some scattering at Middle-Mountain sites LNS-5 and LNS-6, where also a step-like increase in sulfate concentration can be observed. The strong increase in alkalinity in the lower areas indicates their relevance for alkalinity production. Fluoride concentrations are high with considerable variability in the Siwaliks, Middle and High Mountain sampling sites. Chloride, nitrate, and sulfate had highest concentrations during the pre- and post-monsoon season at low elevations. However, in high-elevation sites, the seasonal difference is small or not clearly present, and no clear trend can be observed there (Fig. 2). Nitrate lacks a systematic trend, but elevated concentrations are observed during non-monsoon seasons at the lowest elevation. Sulfate shows a clear seasonality and with locally elevated values at the Middle Mountain sites LNS-5 and LNS-6, particularly during the pre- and post-monsoon seasons.

Among the base cations (Fig. 3), sea-salt corrected sodium $^*Na$ shows the most pronounced seasonality pattern along the entire drainage network, with more than a five-fold lower concentration during the monsoon season than during the pre- and post-monsoon seasons. During the monsoon-season no dilution effect is observed for $^*K$, but in the opposite, elevated concentrations at the lower sites (LNS-1 to LNS-5). Magnesium, and calcium have similar elevational trends for all seasons, interrupted at the Middle Mountain sites (Fig. 3) and show only a small dilution effect during the monsoon season at the lower reaches (LNS-1 to LNS-4).

The contribution from marine aerosols to major ions are ~19.7% for sodium, 1.2% for magnesium, but are negligible for potassium, calcium and sulfate, while the contribution varies with elevation in a not clear, systematic way (Table S2).

The sum of base cations represent an average of the increasing trend with decreasing elevation, with monsoon values lower in a similar manner observed for Na for the silicate derived cations $^*Sbcat_{sil}$, while seasonality is less expressed for cations from carbonate weathering $^*Sbcat_{car}$ (Fig. 3).

4.2. Temporal variability: time series by elevation range

Time series, including interpolations during Nov 2010-Nov 2011, corresponding to four selected elevation sites along the Langtang Narayani river system are presented in Figure S2, Fig. 4 and Fig. 5 (LNS-1 represents Terai, LNS-4 represents Siwaliks, LNS-7 represents Middle

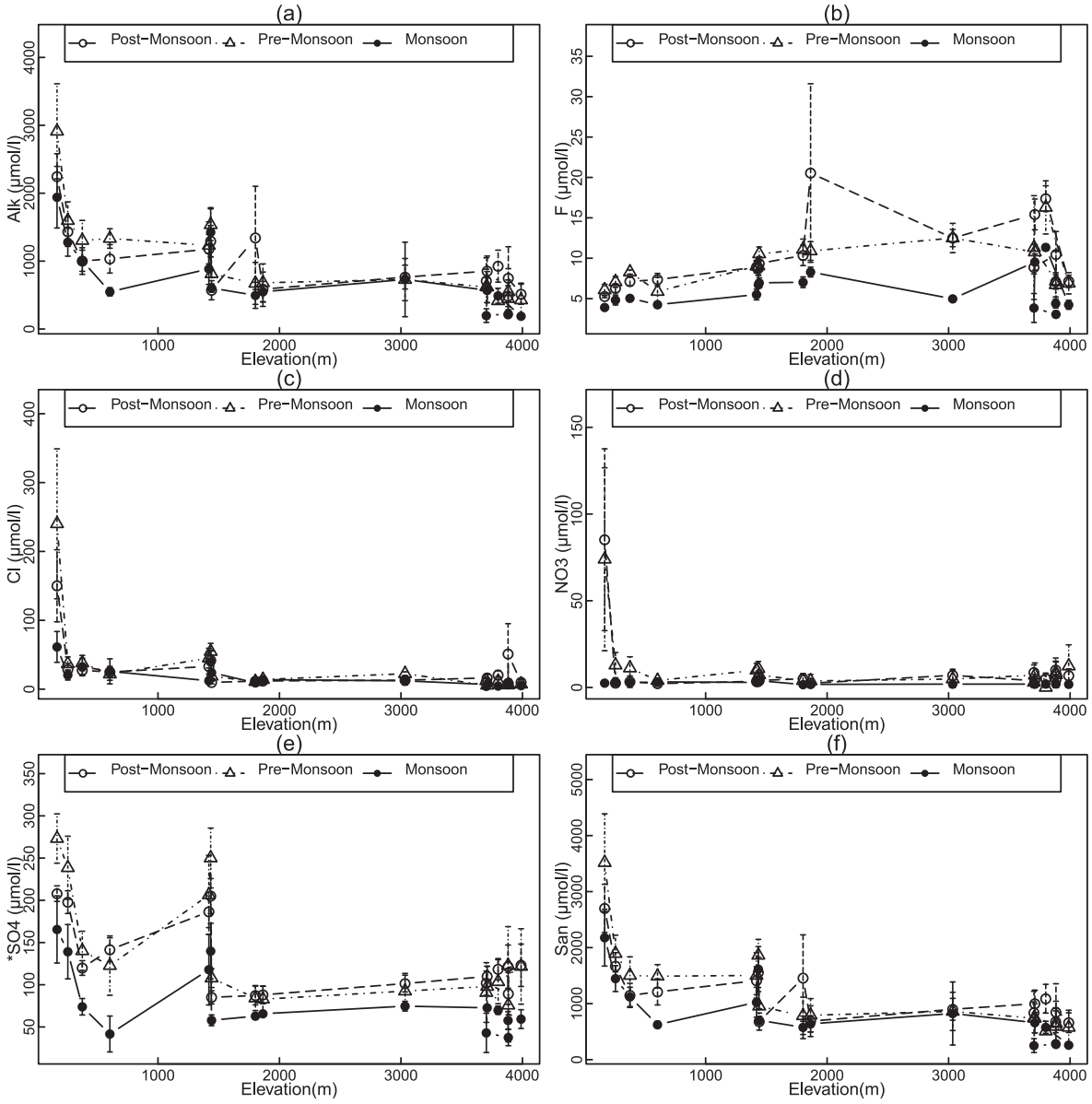

Fig. 2. Elevational gradients by season for major anions and the sum of anions (San) during 2010–2011. Values are averaged for each season and bars correspond to ±standard error.

Mountain, and LNS-11 represents High Mountain). To put the interpretation of concentration patterns in the context of seasonal discharge variation, it should be noted that discharge at all three stations with monitoring data (LNS-1, 4 and 7) decreases from around August/September till April (strongest decrease between August and November) and starts to rise from around May till August with high discharge levels till September.

The pH shows a decreasing pattern towards March 2011, while recovering during the monsoon and post-monsoon season, except for one unusual low value for LNS-7. SS shows a strong increase during the early monsoon season for all stations and prolonged elevated concentrations for the lowest site LNS-1 until September. DOC and TDN show a decreasing pattern until March 2011 for the two lowest sites and then increasing concentrations during the late pre-monsoon and monsoon season (Figure S2d-e). TDN shows an unusually high value in April at LNS-1, which is only in part replicated by NO_3 changes. This lowest sampling site shows in general higher TDN concentrations compared to the others, which is not the case for DOC (Figure S2d-e). Dissolved Si shows a decreasing pattern from January towards the monsoon season, while recovering in during the monsoon and post-monsoon season, with exception of the highest site LNS-11, showing a delayed recovery. There appears to be an increasing concentration pattern towards lower elevations in general for dissolved Si (Figure S2f).

Alkalinity is low during the monsoon season, with exception of LNS-1 (Fig. 4). The alkalinity concentrations

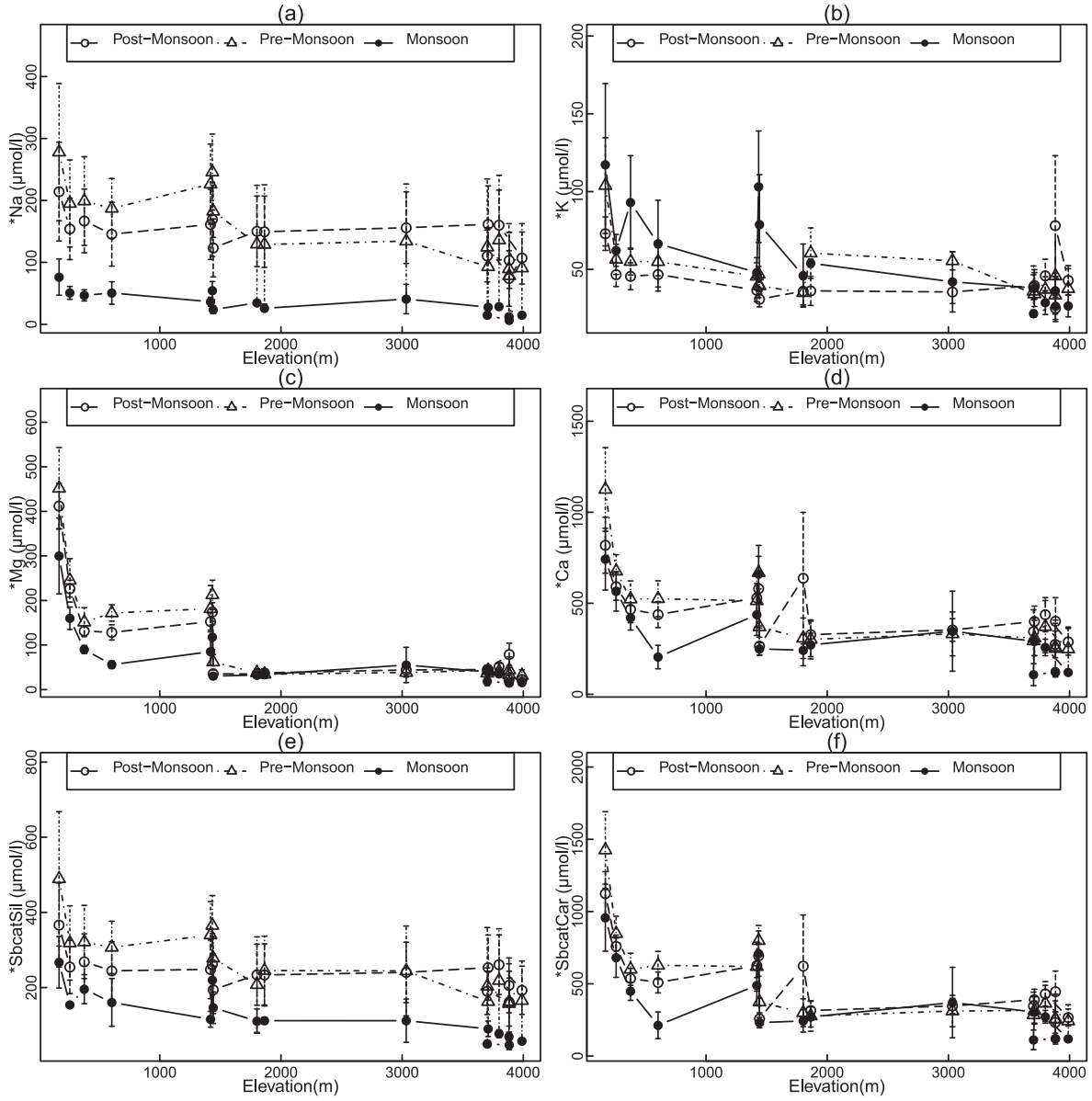

Fig. 3. Elevational gradients by season for major cations and the sum of cations contributed by silicate and carbonate weathering ($^{*}Sbcat_{sil}$ and $^{*}Sbcat_{car}$) during 2010–2011. Values are averaged for each season and bars correspond to ±standard error.

of LNS-1, the lowest elevation sampling location, are distinguishably higher than for the other sites in Fig. 4 throughout the year. F shows the highest concentrations at high elevation during the year, with exception of two data points, and a decreasing trend towards the monsoon season for all stations. Cl, NO_3, and $^{*}SO_4$ at LNS-1 are clearly higher than at the other sampling sites in the pre-monsoon times and for $^{*}SO_4$ during the year with exception of June (Fig. 4).

Sodium shows a comparable pattern for all stations, remaining high during post-monsoon and pre-monsoon and dropping quickly in April/May before the onset of the monsoon considering the discharge records. $^{*}K$ shows a similar trend to $^{*}Na$, except that after the decline in the early monsoon, there is a large concentration pulse (temporal increase) in the middle of the monsoon season for all stations. This pulse is less evident at the high elevation site, suggesting a common process affecting the $^{*}K$ concentration at low to middle elevations during peak discharge time and not causing a dilution effect as observed for $^{*}Na$.

For the cations contributing mostly to the carbonate weathering fluxes ($^{*}Mg$ and $^{*}Ca$) at LNS-1 a comparable concentration pulse can be observed, while dilution might be expected during this period in the monsoon time. This pattern is not observed for the higher sites.

At LNS-1 the observed pulse-like increase in $^{*}Sbcat_{car}$ towards August from carbonate weathering exceeds clearly with about 1,000 µmol L^{-1} relative to the lowest value in June those from base cations $^{*}Sbcat_{sil}$ contributed from silicate weathering with around 150–350 µmol L^{-1} due to increase in $^{*}K$ (depending if choosing May or June as reference point for the increase).

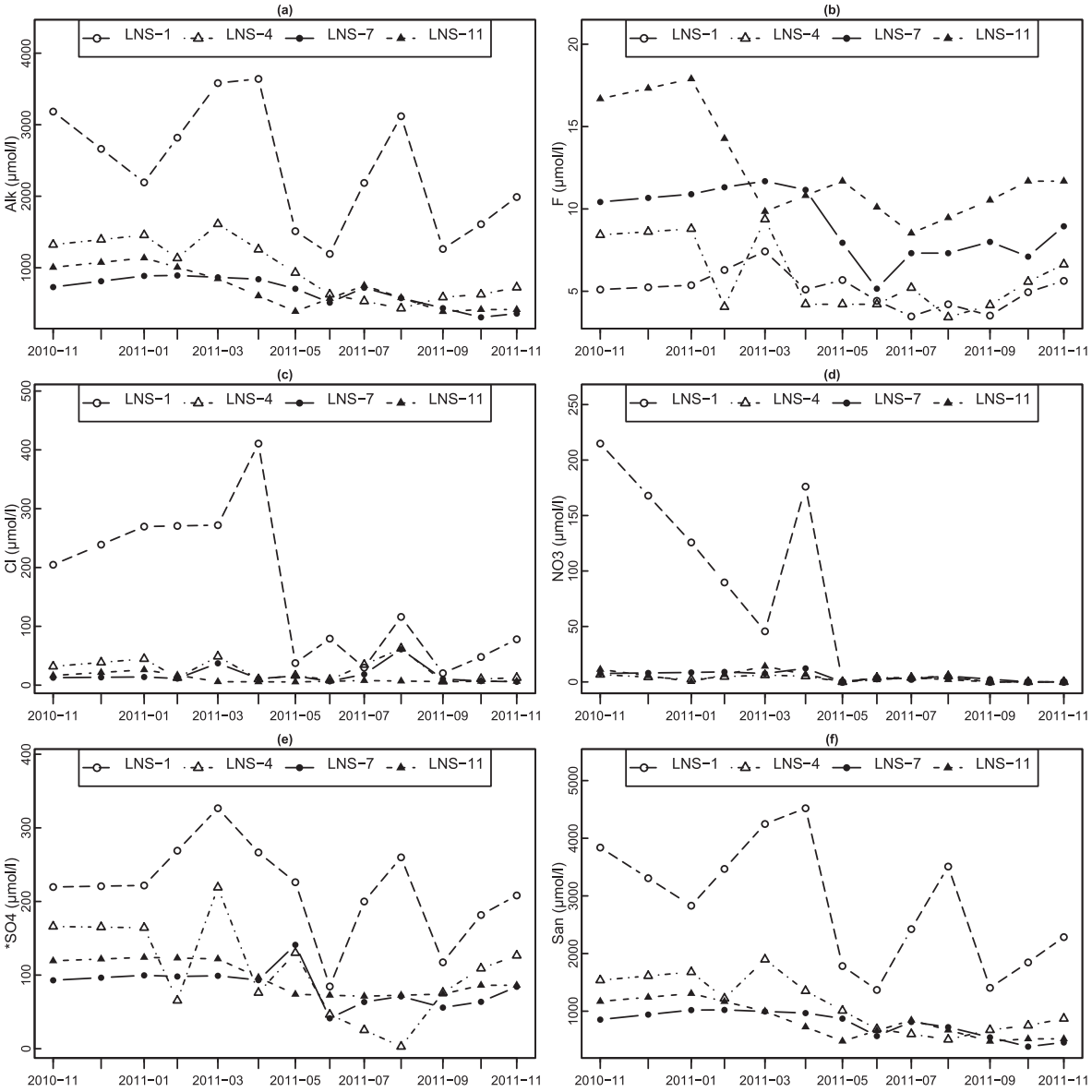

Fig. 4. Time series during Nov 2010-Nov 2011 for representative sampling sites for each elevation range for major anions along the Langtang Narayani river system, including the sum of anions (San). LNS-1 represents Terai, LNS-4 represents Siwaliks, LNS-7 represents Middle Mountain, and LNS-11 represents High Mountain.

For LNS-1 concentrations of *Mg and *Ca are clearly higher on average than at the other sampling sites during the entire year and comparable to the sum of alkalinity and $^{*}SO_4$. In general, the contribution from silicate weathering ($^{*}Sbcat_{sil}$) follows a pattern driven by *Na, *K, and *Mg, whereas contribution of carbonate ($^{*}Sbcat_{car}$) follows the more dominant pattern of *Ca (Fig. 5).

4.3. River water flow and fluxes

River discharge shows the typical seasonal pattern for the region (Fig. 6). Peak monsoon discharge with respect to lowest pre-monsoon discharge is ~8 times larger at Q3, ~30 times larger at Q2, and ~50 times larger at Q1 (locations in Fig. 1). Therefore, the seasonal change in discharge is much more marked at lower elevations than at higher elevations (Fig. 6). Discharge increases at the lower elevation sites are due to inputs from various tributaries such as Kali Gandhaki, Budi Gandhaki, Seti, Bhote Koshi, and Marsyandi. Peak daily flow during the sampling period is 30, 1,143, and 8,607 $m^3 s^{-1}$ for Q3, Q2, and Q1 respectively.

At the Langtang Middle Mountain gauging station (Q3), the average monsoon discharge during the study period was ~20.6 $m^3 s^{-1}$ and 6.3 and 5.1 $m^3 s^{-1}$, respectively, in the post-monsoon and pre-monsoon season. In the Siwaliks section at the Trishuli gauging station at Betrawati (Q2), the average monsoon discharge was ~416 $m^3 s^{-1}$ followed by 57 and 51 $m^3 s^{-1}$, respectively, in the post-monsoon and pre-monsoon season. In the lower Terai plain at the Narayani River gauging station at

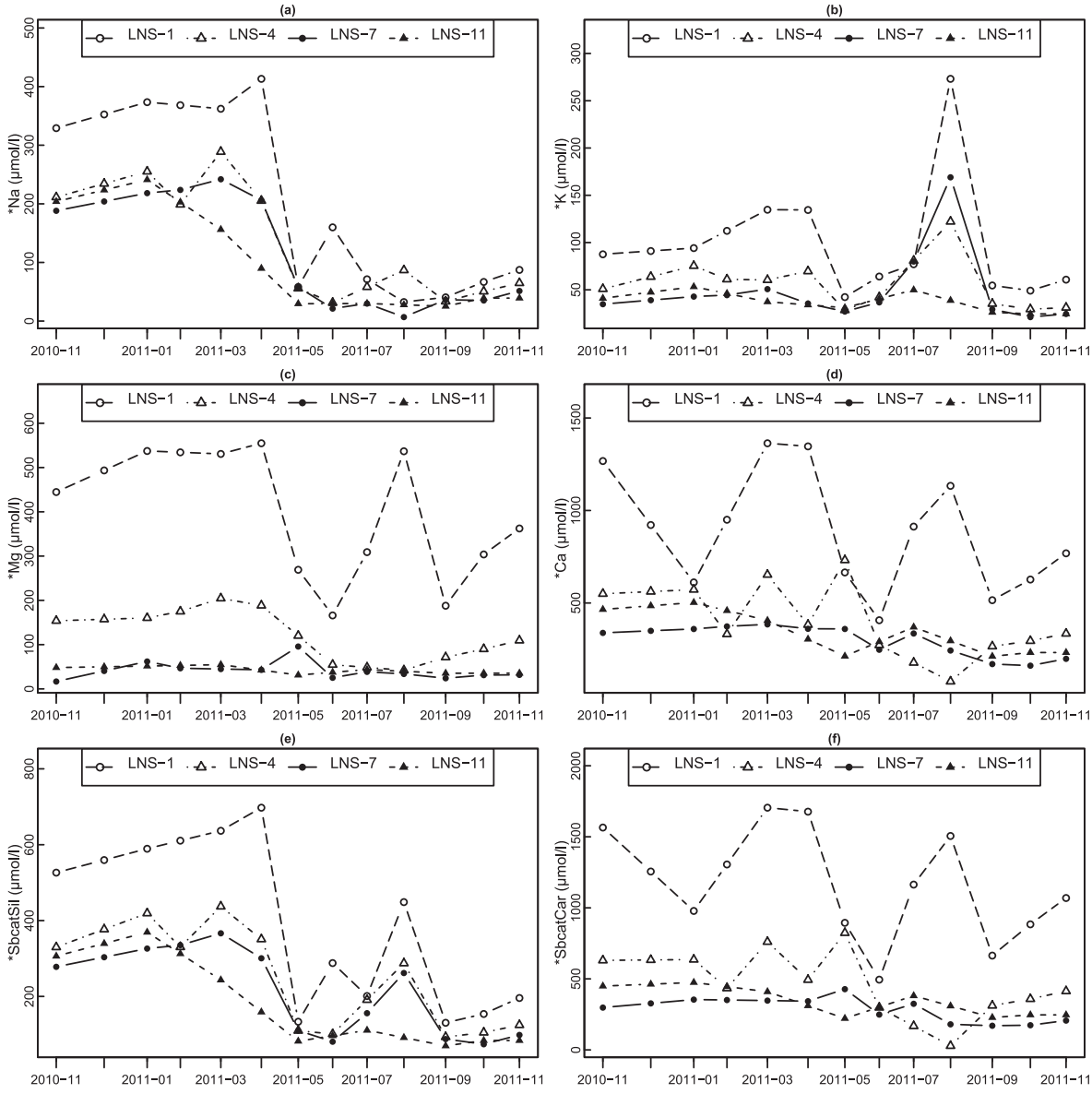

Fig. 5. Time series during Nov 2010-Nov 2011 for representative sampling sites for each elevation range for major cations along the Langtang Narayani river system, including the sum of cations from silicate and carbonate weathering ($^{*}Sbcat_{sil}$ and $^{*}Sbcat_{car}$). LNS-1 represents Terai, LNS-4 represents Siwaliks, LNS-7 represents Middle Mountain, and LNS-11 represents High Mountain.

Narayanghat (Q1), the average monsoon discharge was 3,426 $m^3 s^{-1}$ followed by 350 and 290 $m^3 s^{-1}$ in the post-monsoon and pre-monsoon season respectively.

SS, DOC, TDN concentrations increase with runoff, while less clear for DOC and TDN at LNS-1 (Figure S3), while dissolved Si, anions and cations show in general a typical decreasing concentration with increasing runoff, with exception of NO_3 and Cl at LNS-4 and LNS-7 and less clear for *Mg and *Ca at LNS-7 (Figure S3, Fig. 7 and Fig. 8). As observed above, *K shows for elevated runoff a higher concentration than would be expected from a dilution process (Fig. 8), which is also found for *Ca and *Mg at LNS-1.

We estimated D_w for Si, base cations, sum of base cations (addressing cations originating from carbonate and silicate weathering separately), anions, and sum of anions (Table 4). Dissolved Si has the largest D_w value of 4.08 m/yr for LNS-1 which has a significant p-value of <0.02 and a standard error of 1.42.

At all stations, D_w values for ions or alkalinity originating mostly from carbonate weathering are higher than for *Na and *K contributing to silicate weathering flux. Cl and NO_3 tend to have relative low D_w values at each station compared to chemical species derived from weathering processes, while not always the D_w is statistically significant at $p = 0.05$.

Most of the estimated D_w parameters are characterized by significant p-values ($p < 0.05$), with exception of those with no clear decreasing discharge dilution trend for increasing runoff, as for example NO_3, Cl, K, Ca, and alkalinity at different sampling locations (Table 4, Fig. 7 and Fig. 8).

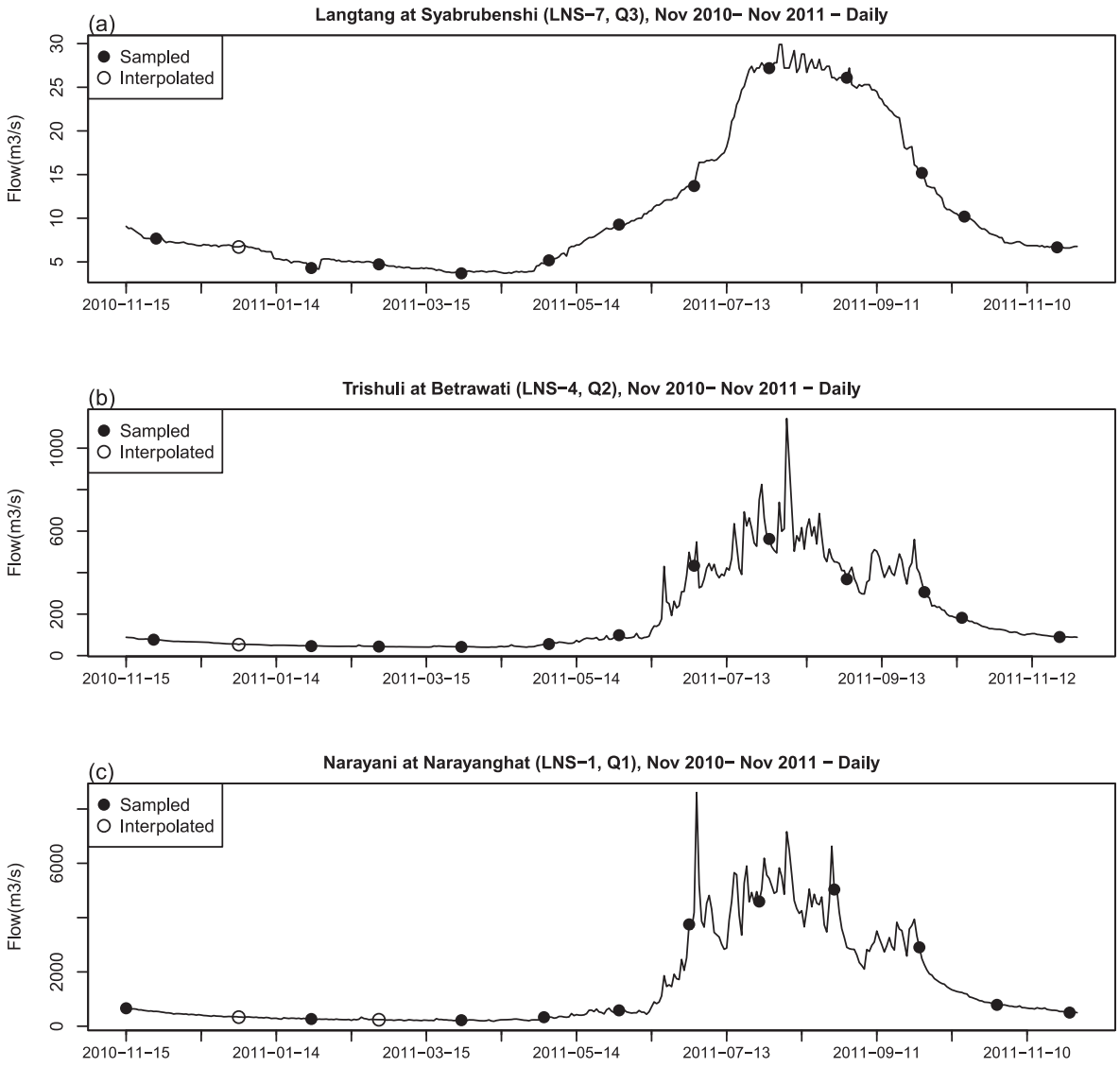

Fig. 6. Daily river water discharge of the Langtang river at Syabrubenshi, Trishuli river at Betrawati, and Narayani river at Narayanghat during the study period Nov 2010-Nov 2011. Circles are the dates of water sampling. In a few cases, values were interpolated.

Resampling using the Monte Carlo method allowed estimating the variability of estimated coefficients C_{max} and D_w for calculated $^{*}Sbcat_{sil}$ and $^{*}Sbcat_{car}$ (Figure S5). In general, C_{max} has distinguishably different values per station, whereas D_w values are similar for LNS-1 and LNS-4 for $^{*}Sbcat_{sil}$ but these two are different from LNS-7. Contrastingly, D_w results for $^{*}Sbcat_{car}$ are similar for LNS-4 and LNS-7 while being different from LNS-1 (Figure S5). The p-values are all below 0.02 except for LNS-1, where most p-values remain below 0.05 but with some values reaching 0.06 (Figure S5).

Flux versus specific discharge analysis show progressively increasing fluxes relative to the increase in runoff, with some exceptions due to clear dilution behavior with increasing runoff as shown above (Figure S4, Fig. 9 and Fig. 10). Most of the measured parameters showed highest fluxes at LNS-1 followed by LNS-4 and LNS-7 except for nitrate (Figure S4, Fig. 9 and Fig. 10).

4.4. Annual export of measured chemical parameters

Annual area normalized exports of solutes (Table 5) showed highest rates at the low elevation site Narayanghat (Q1, LNS-1), and lower exports at station Q2 (LNS-4) and Q3 (LNS-7), in general. However, DOC export rates are somewhat higher at the mid-mountain site LNS-4 than at the lower site LNS-1 (Table 5).

Annual export rates for most parameters were highest during the monsoon season, while the annual contributions from the post-monsoon and pre-monsoon seasons were in general comparable to each other (Table 5). Of the major chemical species $^{*}Na$ is an exception, with lower export rates during the monsoon season compared to the two other seasons at the highest discharge monitoring site Q3 (LNS-7). The monsoon period is most relevant for the parameter SS, as the monsoon season contribution to the annual fluxes are ~99%, 98%, and 97% for Q1, Q2, and Q3, respectively.

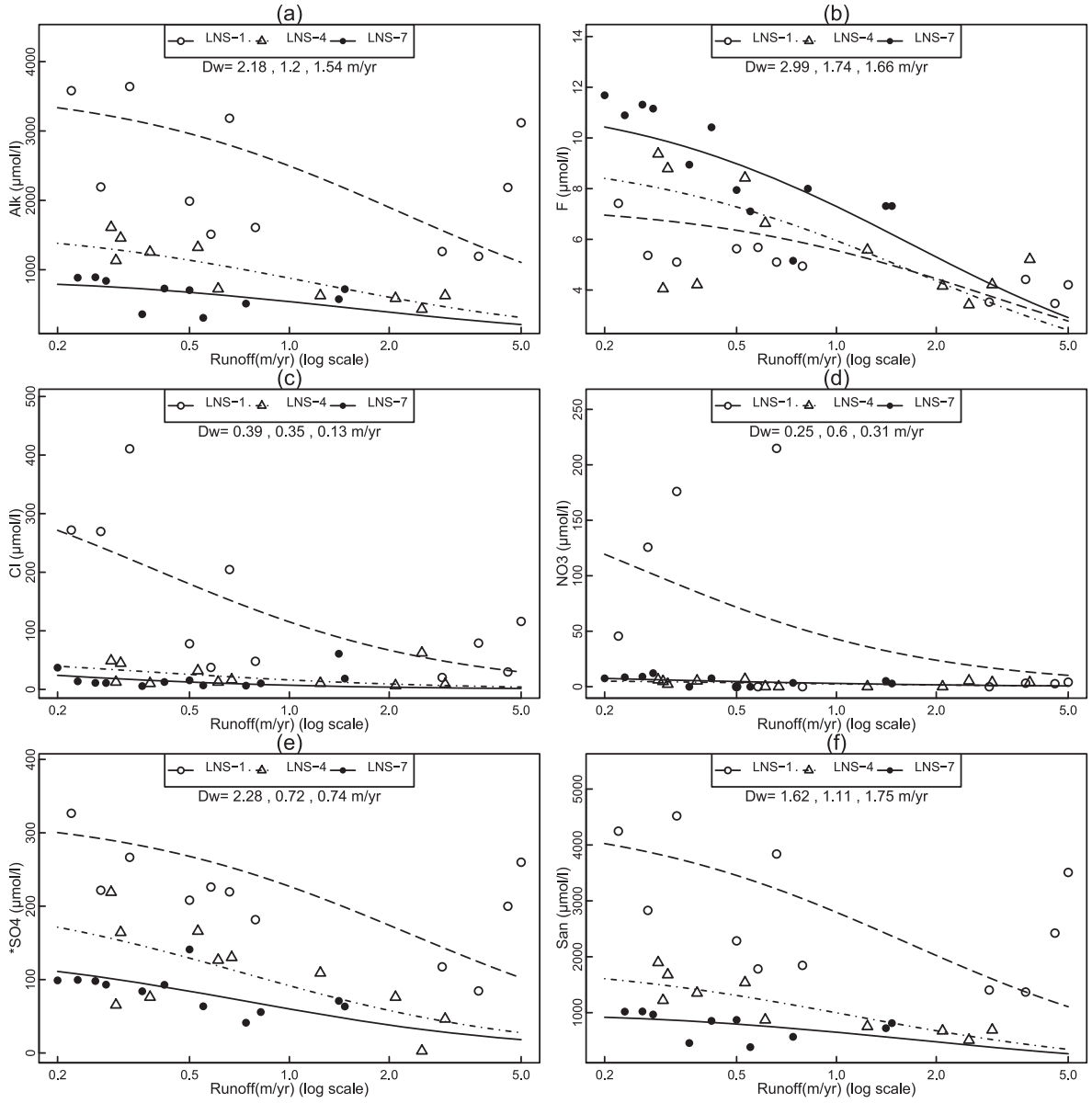

Fig. 7. Concentration vs. specific discharge (runoff) for major anions for each station with discharge data and fit of the Maher and Chamberlain equation and the values of the Damköhler coefficient D_w in m/yr.

At Q1, the monsoon contribution to the export rate is above 70% for most dissolved parameters (exceptions are Cl and *Na, and NO_3, with only ~20%; Table 5). A lower contribution of the monsoon fluxes to the annual export rate is observed at the stations Q2 and Q3 compared to Q1, on average.

5. DISCUSSION

5.1. General patterns

Many of the measured parameters showed an increase in concentrations with decreasing elevation along the river system, with a break at LNS-5 (1,419 m asl) and LNS-6 (1,434 m asl) because of the mixing of the Bhotekoshi with the Langtang at Syabrubenshi (Figure S1, Fig. 2 and Fig. 3). These sites (LNS-5 and LNS-6) situated at the MCT region where pCO_2 is comparatively high, and correlated with elevated levels of sulfate, calcium and alkalinity and lower pH (Table 3 and Table S1). Latter observations were previously linked to sulfide oxidation and carbonate dissolution, while from sub-catchments metamorphic CO_2 may contribute to the observed alkalinity fluxes (Galy and France-Lanord, 1999; France-Lanord et al., 2003; Evans et al., 2008; Wolff-Boenisch et al., 2009; Bhatt et al., 2016).

DOC concentration did not show a clear elevation trend, but elevated values occurred at a landslide site location, LNS-10. The DOC concentration, in general <250 µmol L^{-1}, is below the average of the median of

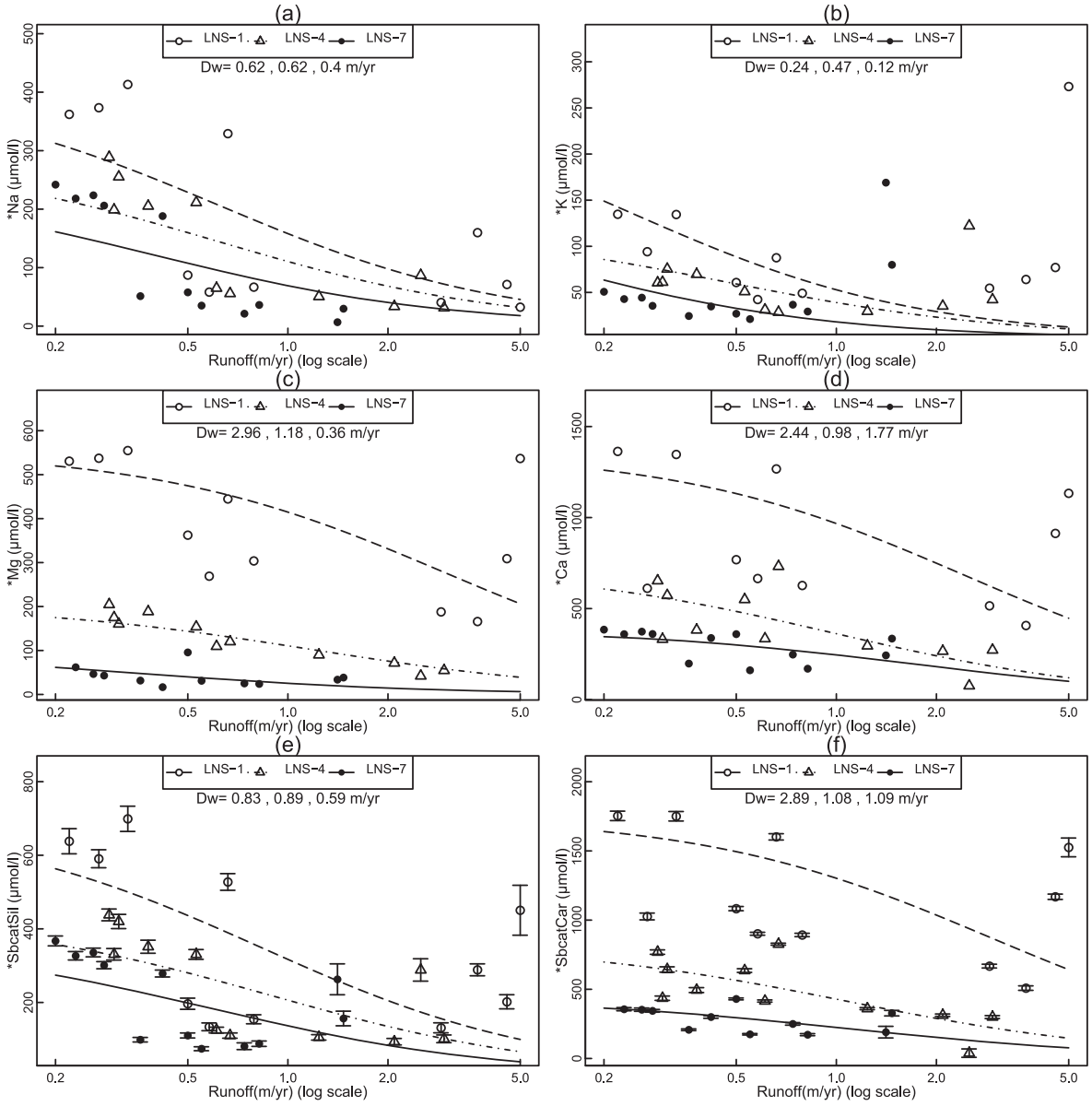

Fig. 8. Concentration vs. specific discharge (runoff) for major cations for each station with discharge data and fit of the Maher and Chamberlain equation and the values of the Damköhler coefficient D_w in m/yr.

6,772 catchments reported in the GLORICH database with 395 µmol L^{-1}, but closer to the 257 µmol L^{-1} if only catchments with elevation above 500 m (n = 2,217) are selected (Hartmann et al., 2014). The export rates of DOC from the Middle Mountain area and low elevation sites were 3.33 and 2.62 tons km^{-2} yr^{-1}, respectively and higher than that of some North American River basins, but lower than that of small tropical mountain rivers in Panama (Lauerwald et al., 2012; Goldschmidt et al., 2015). Global DOC fluxes vary in general between 0.1 ton C km^{-2} yr^{-1} and 14 tons C km^{-2} yr^{-1} (Aitkenhead and McDowell, 2000).

Human population density and activities such as agriculture may have some impact on low elevation hydrochemistry, and specifically TDN concentrations during post-monsoon season from LNS-1 to LNS-4. This is not reflected in the nitrate concentrations, with exception of lower N-values at LNS-1, suggesting elevated contributions from DON (not measured) or ammonium. Livestock activities may have some impact on high elevation sites relative to the middle section of the basin (Collins and Jenkins, 1996; Bhatt et al., 2009), and nitrate or TDN levels are within the global range of elevated catchments (compared with GLORICH data in Hartmann et al., 2014).

5.2. Geogenic controls

The sea-salt contribution of sulfate is small along the drainage network, suggesting that most sulfate is from geogenic sources along the studied drainage network (Galy and

Table 4
Statistics of non-linear regression estimates for C_{max} and D_w for all ionic species. The columns for $^{*}Sbcat_{sil}$ and $^{*}Sbcat_{car}$ are for the calculated mean values. Their variability is further explored by Monte Carlo analysis (see Figure S5).

Station	Coeff or statistic	Alk μmol/l	F μmol/l	Cl μmol/l	NO_3 μmol/l	SO_4 μmol/l	*Na μmol/l	*K μmol/l	*Mg μmol/l	*Ca μmol/l	Si μmol/l	San μmol/l	*Sbcat μmol/l	$^{*}Sbcat_{sil}$ μmol/l	$^{*}Sbcat_{car}$ μmol/l
LNS-1	Cmax (μmol/l)	3,641	7	411	215	327	413	273	555	1,364	215	4,521	2,450	698	1,705
	Dw (m/yr)	2.18	2.99	0.39	0.25	2.28	0.62	0.24	2.96	2.44	4.08	1.62	1.94	0.83	3.05
	Dw std err (m/yr)	1.04	0.73	0.13	0.13	0.84	0.25	0.13	1.31	1.22	1.42	0.71	0.86	0.37	1.44
	Dw p-value	0.061	0.002	0.015	0.095	0.022	0.03	0.097	0.048	0.073	0.017	0.045	0.048	0.047	0.06
	Residual Std Err (μmol/l)	1,033	1	91	70	72	108	89	143	403	42	1,211	656	201	465
	Degrees of freedom	10	10	10	10	10	10	10	10	10	10	10	10	10	10
LNS-4	Cmax (μmol/l)	1,611	9	62	7	219	289	122	205	732	255	1,897	1,207	437	823
	Dw (m/yr)	1.2	1.74	0.35	0.6	0.72	0.62	0.47	1.18	0.98	0.69	1.11	1.14	0.89	1.07
	Dw std err (m/yr)	0.24	0.56	0.17	0.33	0.22	0.17	0.19	0.18	0.28	0.29	0.22	0.22	0.29	0.29
	Dw p-value	0.001	0.011	0.068	0.096	0.007	0.005	0.036	0	0.006	0.034	0.001	0	0.012	0.005
	Residual Std Err (μmol/l)	204	2	21	3	47	58	36	21	147	77	239	156	100	156
	Degrees of freedom	9	10	10	11	10	10	10	10	10	11	9	10	10	10
LNS-7	Cmax (μmol/l)	893	12	61	12	141	242	169	96	385	121	1,023	689	367	428
	Dw (m/yr)	1.54	1.66	0.13	0.31	0.74	0.4	0.12	0.36	1.77	1.69	1.75	1.2	0.59	1.07
	Dw std err (m/yr)	0.61	0.32	0.07	0.12	0.16	0.14	0.06	0.11	0.59	0.38	0.7	0.38	0.2	0.3
	Dw p-value	0.032	0	0.072	0.03	0.001	0.014	0.083	0.009	0.012	0.001	0.033	0.011	0.012	0.005
	Residual Std Err (μmol/l)	206	1	19	4	23	65	52	22	78	17	227	149	96	83
	Degrees of freedom	9	11	11	10	11	11	11	10	11	11	9	10	11	10

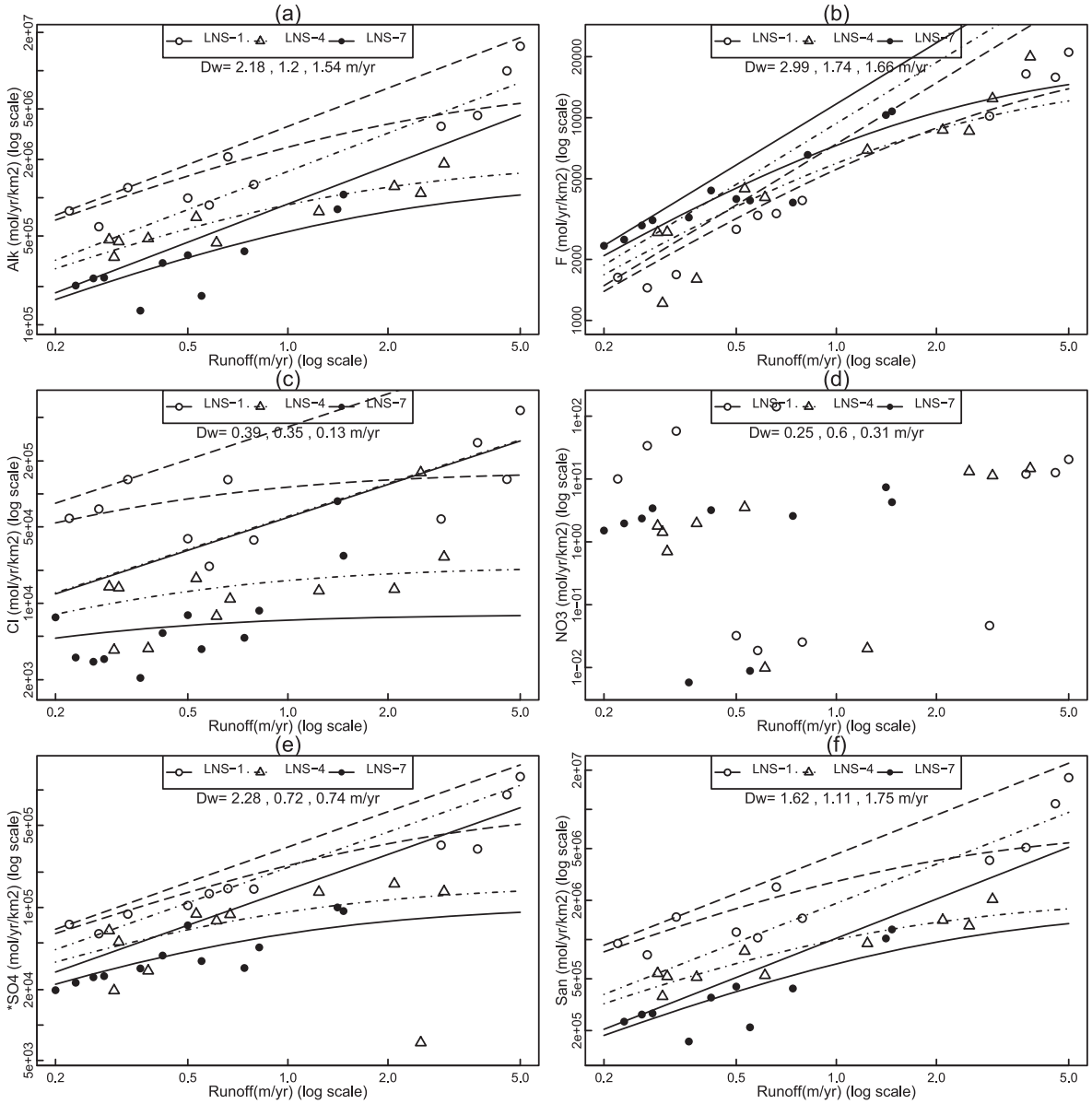

Fig. 9. Flux vs. specific discharge (runoff) for major anions. Shown for each station, are the fit of the Maher and Chamberlain equation (curves) and the straight lines corresponding to the C_{max} or thermodynamic limit.

France-Lanord, 1999; Bhatt et al., 2007). The oxidation of pyrites produces sulphuric acid and dissociates into sulfate and protons, while iron is precipitated as iron (III)-hydroxides/oxides, e.g. (Drever 1988):

$$FeS_2 + 3.75O_2 + 3.5H_2O \rightarrow Fe(OH)_3Precip + 2SO_4^{2-} + 4H^+ \quad (13)$$

In the presence of produced sulphuric acid from pyrite oxidation, the weathering rate can be enhanced and CO_2-fluxes into the critical zone can have locally less influence on weathering fluxes:

$$CaCO_3 + H_2SO_4 \rightarrow Ca^{2+} + SO_4^{2-} + CO_2\uparrow + H_2O \quad (14)$$

or

$$2CaCO_3 + H_2SO_4 \rightarrow 2Ca^{2+} + 2HCO_3^- + SO_4^{2-} \quad (15)$$

The annual basin export ratios of alkalinity to sea-salt corrected sulfate is 5.7 for the study area and the exported sulfate equivalents are as high as the base cation equivalents from silicate weathering (98%), because of the high calculated carbonate to silicate weathering ratio. Therefore, an idealized silicate CO_2-consumption rate of the basin assuming that silicate derived base cations are counterbalanced by alkalinity would compensate for the pyrite oxidation in the studied central Himalaya region (c.f. Galy and France-Lanord, 1999).

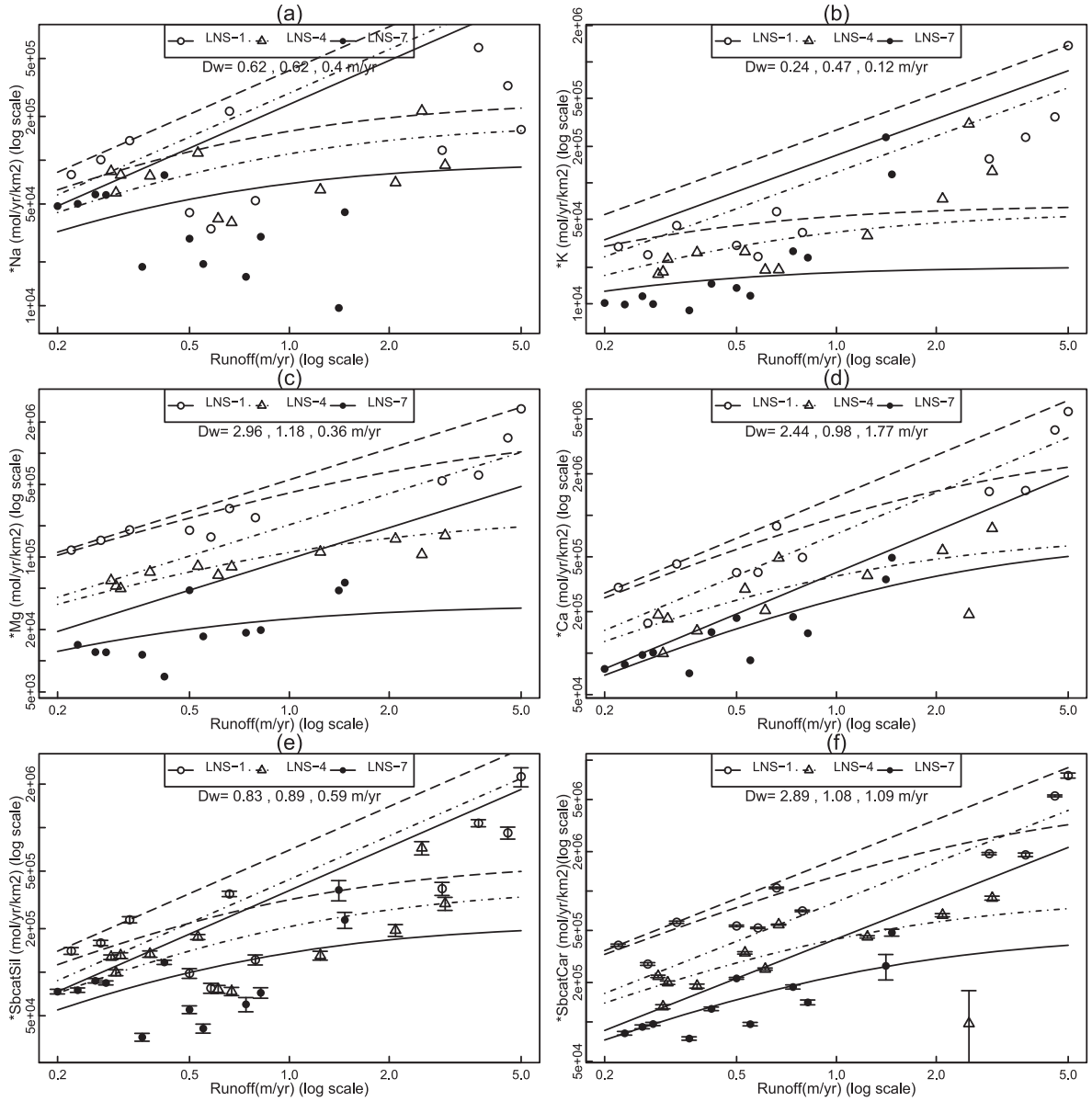

Fig. 10. Flux vs. specific discharge (runoff) for major cations. Shown for each station, are the fit of the Maher and Chamberlain equation (curves) and the straight lines corresponding to the C_{max} or thermodynamic limit.

This finding could be extended by seasonal analysis of sulfur isotopes to test the proposed contribution of sulfur oxidation to weathering fluxes. In general, the oxidation of sulfides can be relevant for weathering rates of affected basins (e.g., Calmels et al., 2007). Sulfide oxidation can also be a cause for substantial CO_2-degassing from the water (Torres et al., 2016, 2017). Note that clearly elevated pCO_2 values can be observed below station LNS-7 (Fig. 12a), spatially correlated with an increase in sulphate concentration and drop in pH. The observed step like change in water chemistry appears when the river enters the Lesser Himalayan sediment area below LNS-7. This region crosses the MCT after mixing with the Bhotekoshi at Syabrubensi. Its basin contains a significant proportion of sulfide bearing minerals and carbonates (e.g., Galy and France-Lanord, 1999; Bhatt et al., 2009). The dominance of calcium, sulfate and alkalinity along the drainage network supports the model that sulfide oxidation coupled with carbonate dissolution are dominant geochemical processes for weathering flux production (Galy and France-Lanord, 1999). In addition to these processes, higher concentrations of major solutes particularly within the MCT region attributed to metamorphic activities and the presence of hot springs and changes in lithology were reported (Evans et al., 2008). The latter study described the presence of numerous hot springs discharging into the flowing streambeds at the foot of the high Himalaya near the MCT region. Evans et al. (2008) found that the Himalayan metamorphic processes provide a source of CO_2, which is larger than the consumption of CO_2 by

Table 5
Annual river runoff and export of water constituents for each of the three stations with discharge data. Percentage of runoff and export by season is also reported for each station.

	Units	LNS-1 Total	LNS-1 Pre (%)	LNS-1 Mons (%)	LNS-1 Post (%)	LNS-4 Total	LNS-4 Pre (%)	LNS-4 Mons (%)	LNS-4 Post (%)	LNS-7 Total	LNS-7 Pre (%)	LNS-7 Mons (%)	LNS-7 Post (%)
Runoff	m yr^{-1}	1.45	6.53	78.59	14.88	1.27	9.02	73.23	17.75	0.60	15.06	62.31	22.63
SS	ton km^{-2} yr^{-1}	1,611	0.48	99.41	0.11	613.29	0.61	98.12	1.27	333.92	1.77	96.80	1.43
DOC	ton km^{-2} yr^{-1}	2.62	7.11	84.61	8.25	3.33	4.59	81.18	14.25	0.85	16.29	72.27	11.70
TDN	ton km^{-2} yr^{-1}	1.40	11.89	73.08	14.68	0.77	4.98	60.62	34.34	0.17	13.38	70.71	13.26
SiO_2	ton km^{-2} yr^{-1}	12.72	7.75	79.28	13.01	9.96	9.20	75.42	15.34	2.95	19.77	51.92	28.31
Alk	mol km^{-2} yr^{-1}	3,367,795	8.73	82.13	9.13	848,632	18.53	59.99	21.48	362,379	22.51	59.27	18.23
F	mol km^{-2} yr^{-1}	6,710	10.04	77.82	12.14	6,171	11.15	66.09	22.76	4,722	21.51	54.82	23.67
Cl	mol km^{-2} yr^{-1}	130,221	17.99	67.55	14.46	33,812	7.96	79.98	12.06	13,321	13.12	78.21	8.67
NO_3	mol km^{-2} yr^{-1}	18,550	40.12	20.05	39.82	3,839	11.11	83.74	5.15	2,354	25.42	57.18	17.40
$^{*}SO_4$	mol km^{-2} yr^{-1}	296,285	9.95	79.49	10.56	76,207	21.54	43.04	35.42	44,085	26.46	50.39	23.15
San	mol km^{-2} yr^{-1}	3,826,353	9.31	81.10	9.59	966,204	17.97	59.76	22.27	429,386	22.41	59.20	18.40
$^{*}Na$	mol km^{-2} yr^{-1}	152,577	18.41	64.67	16.93	93,252	22.86	53.09	24.06	37,452	42.27	21.82	35.91
$^{*}K$	mol km^{-2} yr^{-1}	194,396	5.36	89.36	5.28	82,132	8.18	81.41	10.41	40,914	9.06	81.93	9.01
$^{*}Mg$	mol km^{-2} yr^{-1}	540,196	8.97	79.92	11.11	95,019	22.90	52.03	25.08	23,194	28.75	50.68	20.57
$^{*}Ca$	mol km^{-2} yr^{-1}	1,278,464	8.82	82.49	8.69	338,947	22.49	54.03	23.48	163,435	22.87	58.38	18.75
*Sbcat	mol km^{-2} yr^{-1}	2,165,633	9.22	81.21	9.57	609,350	20.68	57.26	22.06	264,084	23.73	56.37	19.90
$^{*}Sbcat_{sil}$	mol km^{-2} yr^{-1}	474,686	10.39	79.83	9.77	235,100	15.17	67.93	16.91	106,312	23.10	56.52	20.39
$^{*}Sbcat_{car}$	mol km^{-2} yr^{-1}	1,667,272	8.76	81.80	9.44	368,102	24.42	50.07	25.51	156,228	24.75	55.61	19.64
Sbcat	mol km^{-2} yr^{-1}	2,295,554	9.72	80.44	9.84	999,488	12.88	73.27	13.85	276,946	23.10	57.50	19.39
DIC	mol km^{-2} yr^{-1}	1,940,186	6.66	86.53	6.82	583,659	34.06	53.50	12.45	216,266	24.58	51.97	23.45
CO_2	mol km^{-2} yr^{-1}	84,034	16.60	80.12	3.29	146,172	93.76	3.85	2.39	87,978	21.27	48.64	30.09
HCO_3	mol km^{-2} yr^{-1}	1,804,808	6.19	86.86	6.96	428,639	14.23	69.91	15.86	126,847	26.95	54.06	18.99
CO_3	mol km^{-2} yr^{-1}	7,509	5.53	83.98	10.48	2,882	1.20	85.69	13.11	449	3.84	89.23	6.93
*Sbcat (mass)	ton km^{-2} yr^{-1}	75.48	8.94	81.91	9.15	21.25	20.41	57.85	21.74	9.55	22.41	58.72	18.82
Sbcat (mass)	ton km^{-2} yr^{-1}	78.56	9.30	81.35	9.36	35.70	12.33	74.48	13.21	9.85	22.04	59.44	18.53
W_D^e	mm kyr^{-1}	201.12	8.94	81.91	9.15	56.62	20.41	57.85	21.74	25.45	22.41	58.72	18.82

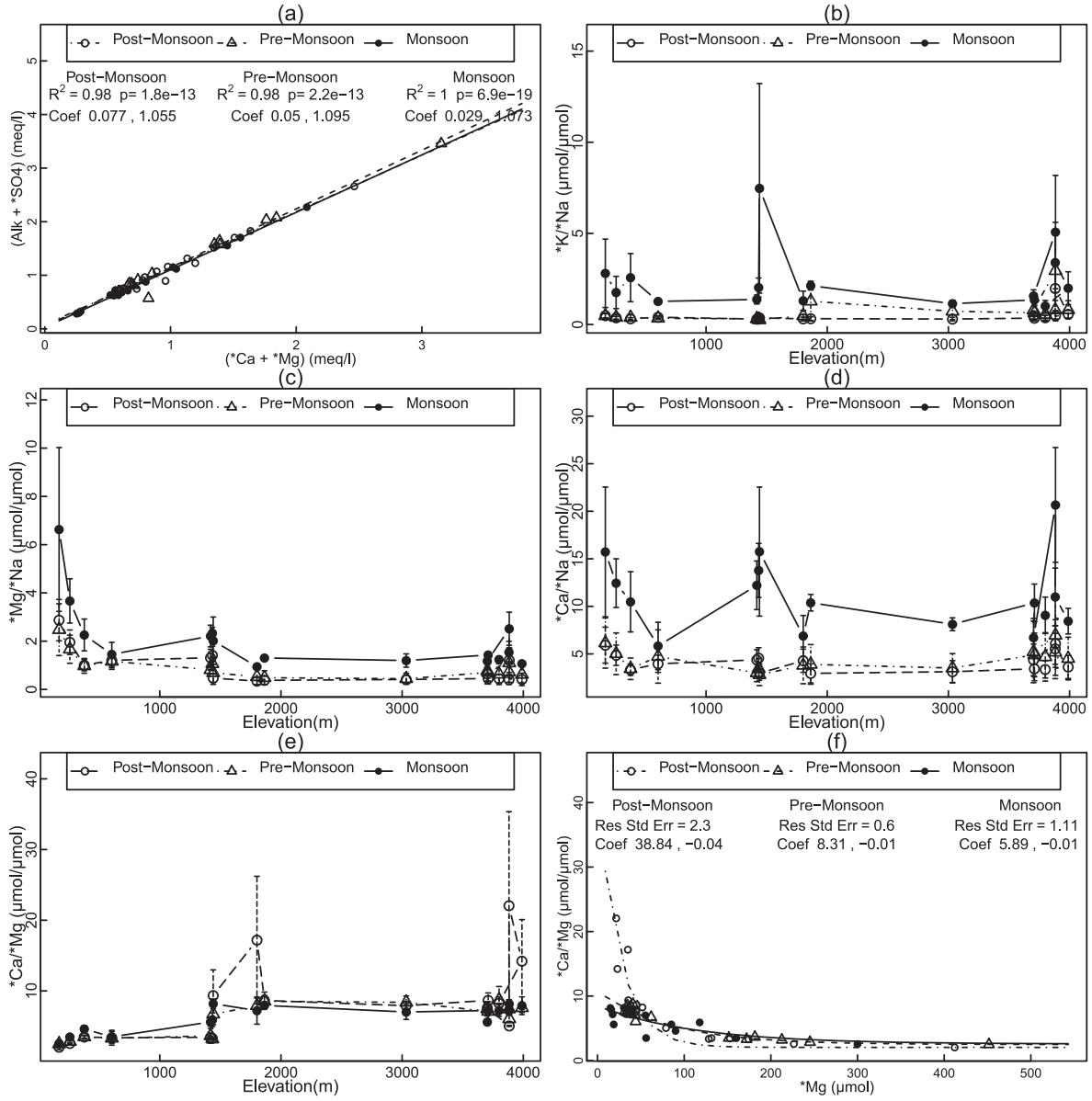

Fig. 11. Relationships between major anions and cations, and molar ratios with elevation. (a): Relationship between sum of alkalinity and sulfate versus sum of calcium and magnesium after sea-salt correction by season. (b–d): Gradients by season of molar ratios of $^{*}K/^{*}Na$, $^{*}Mg/^{*}Na$, and $^{*}Ca/^{*}Na$. (e) Gradient by season of molar ratios of $^{*}Ca/^{*}Mg$ (f): Relationship between $^{*}Ca/^{*}Mg$ and $^{*}Mg$.

weathering of Himalayan basins. The drop in pH towards the MCT region is therefore not only affected by sulfide oxidation but also by geogenic CO_2 sources linked with metamorphic activities. Their contribution could not be quantified here, and some of the excess CO_2 may degas. While sulfide oxidation appears within the whole drainage basin, the influences of metamorphic processes seem locally or regionally constrained (c.f., Evans et al., 2008). The sum of sea-salt corrected sulfate and alkalinity equivalents has a quasi 1:1 linear relationship with the sum of sea-salt corrected calcium and magnesium equivalents ($R^2 \sim 1$ for all seasons in Fig. 11a), which supports the interpretation.

The relatively higher contribution of chemical weathering rates from carbonates is in accordance with previous reports suggesting a dominant role of carbonate weathering over the silicate weathering in the Himalayan landscape (Table 5, Sarin et al., 1989; Bhatt et al., 2000; Dalai et al., 2002; France-Lanord et al., 2003; Wolff-Boenisch et al., 2009).

5.3. Seasonal dynamics

Some measured chemical species along the drainage network exhibit seasonal changes in concentration. In general, lowest concentrations of dissolved species are observed during the monsoon season, due to dilution, whereas higher concentrations occur in the pre-monsoon and post-monsoon seasons. Unlike dissolved chemical species, suspended sediment was highest during the monsoon season; high sediment transport and erosion rate from the

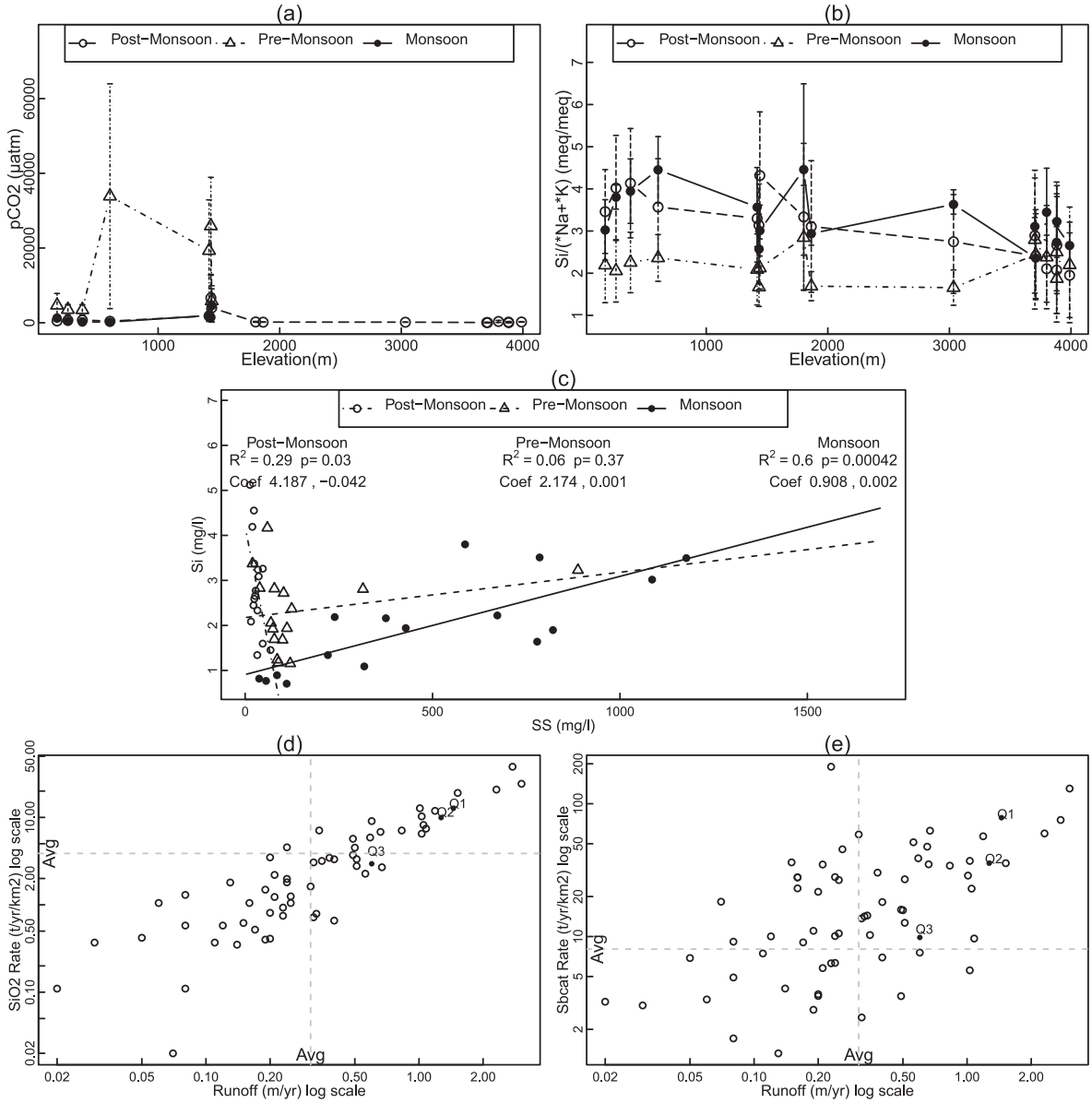

Fig. 12. (a): Variation of pCO_2 in surface waters of Langtang-Narayani river system as a function of elevation. (b) Ratios of dissolved silicon to sum of sodium and potassium after sea-salt correction as a function of elevation and by season. (c): dissolved silicon versus suspended sediment by season. (d): Comparison of runoff versus dissolved SiO_2 load of Q1, Q2, and Q3 with the average of major rivers of the World. (e): Comparison of runoff versus sum of base cation (Sbcat) load of Q1, Q2, and Q3 with the average of major rivers of the world. Q1, Q2, and Q3 represent discharge measurement sites at Narayani river at Narayanghat, Trishuli river at Betrawati and Langtang river at Syabrubenshi respectively (Fig. 1).

Himalayan catchment is known to occur during the intense Asian monsoon (Bookhagen, 2010). Roback et al. (2018) pointed out that not all the landslide materials reached the stream channel after a seismic event, but a relevant amount is transported later, especially during the monsoon.

Seasonality of major dissolved species can be summarized using the sum of cation and anion patterns. Besides the seasonal dilution concentration cycle, the concentration rise and decline of dominant species (i.e., Alk, $^{*}SO_4$, $^{*}Ca$, $^{*}Mg$, Si) around August, during the monsoon season, represents a monsoonal concentration pulse, which is probably related to the mobilization and drainage of soil-rock water with elevated concentrations. This pulse must be high enough to compensate for a dilution effect during high flow conditions. Some of the fluids being mobilized may be due to enhanced landslide activity (c.f. Jin et al., 2016) within the Himalayan landscape during wet monsoon periods (Gabet et al., 2004), adding to elevated weathering fluxes during this season.

5.4. Concentration-discharge relationships

All three gauging stations (Q1, Q2, and Q3) showed strong discharge seasonality affecting the seasonality of

the concentrations and fluxes. The high D_w value at LNS-1 is consistent with elevated concentrations during the monsoon time when compared to other sites. Catchments with higher D_w values, such as those in rapidly eroding mountains, can be interpreted to be more efficient at generating solutes and elevated C_{max} concentration (Maher and Chamberlain, 2014; Ibarra et al., 2016).

The variability of estimated values of coefficients C_{max}, D_w for calculated $^{*}Sbcat_{car}$ and $^{*}Sbcat_{sil}$ is modest relative to the estimated values for each discharge station (Figure S5). Estimated values of coefficient C_{max} are significantly different among sampling locations, showing an increasing trend with decreasing elevation for both silicate and carbonate related cation contents. However, the coefficient D_w differs when comparing silicate or carbonate weathering products. For silicate $^{*}Sbcat_{sil}$, the values of D_w are similar for LNS-1 and LNS-4 but these two are different from LNS-7. Contrastingly, for carbonates $^{*}Sbcat_{car}$, D_w values are similar for LNS-4 and LNS-7 but these two are lower than that for LNS-1 (Figure S5).

The Si-D_w value for LNS-1 is 4.08 m/yr higher than the mean Si-D_w value of 3.47 m/yr identified for basaltic catchments and much higher than the mean Si-D_w value of 1.49 m/yr for granitic catchments (c.f., Ibarra et al., 2016), suggesting intense weathering at the base of the Himalaya with respect to silica mobilization. Higher D_w values at the base of the Himalaya for both $^{*}Sbcat_{car}$ and $^{*}Sbcat_{sil}$ (Figure S5) are probably due to the combination of higher reaction rates and flow paths properties (Maher and Chamberlain, 2014). Intense weathering reactions in these areas are due to favorable climatic conditions, reactivity of minerals and hydrologic properties of the soil-rock system at the lower elevation region.

5.5. Elemental ratios of weathering products

In order to further interpret weathering controlling factors, we calculated several ratios and relationships among weathering products. The molar ratios of $^{*}K/^{*}Na$, $^{*}Mg/^{*}Na$ and $^{*}Ca/^{*}Na$ show seasonal patterns (Fig. 11 b, c, and d, respectively) with elevated ratios during the monsoon across the elevation range. This reflects that during the wetter conditions Na concentrations were more diluted (compare Fig. 11 with Fig. 3) and that this dilution effect was weaker or absent for the other three elements, dependent on timing. The declining ratios of ($^{*}Ca/^{*}Mg$) towards low elevations in the Langtang-Narayani river system is caused by a stronger increase in Mg-concentrations (Fig. 11e). Using an exponential model $y = y_0\exp(-kx) + y_{min}$, the molar ratio of $^{*}Ca/^{*}Mg$ (variable y) decreases with increasing $^{*}Mg$ concentration (variable x) with a higher decay constant ($k = 0.04$) for the post-monsoon season compared to the pre-monsoon ($k = 0.01$) and monsoon period ($k = 0.01$) (Fig. 11f). This suggests that mobilization of $^{*}Ca$ and $^{*}Mg$ might be differently affected by seasonal controls.

An additional process to partly explain the decreasing pattern in the $^{*}Ca/^{*}Mg$ ratio towards lower elevation sites is instream calcite precipitation as was suggested for the Himalayan drainage network (Galy and France-Lanord, 1999; Dalai et al., 2002; Bickle et al., 2018).

There is a seasonal variation of the ratio of dissolved Si to sum of sodium and potassium after sea-salt correction along the river system, suggesting a seasonal control on incongruent release rates of Si versus K and Na from the system, when the monsoon and post-monsoon periods are compared with the pre-monsoon period (Fig. 12b). This may be due to differences in mobilization processes, and sources of dissolved silica in the river. For example, silica is also mobilized from the soil system, as silica can accumulate in the upper soil horizons significantly via the biological pump (Struyf and Conley, 2011).

5.6. Chemical weathering and physical erosion

High export rates of weathering products from river systems originating in the central Himalaya are due to high runoff and steep relief (~4 km elevation drop in ~150 km distance). This is evident in the high suspended sediment flux (Figure S4, Table 5), with its strong runoff dependency due to seasonal control. The relationship between physical erosion based on SS and silicate chemical weathering fluxes is ambivalent. For example, a linear regression between dissolved Si concentration and SS concentration shows modest R^2 and statistically significant trend ($R^2 = 0.6$ and $p < 0.0004$) during the monsoon but much weaker and lacking significance for other seasons (Fig. 12c). In general, there is a dilution trend with increasing runoff for the sum of silicate cations (Fig. 8), while the opposite occurs for the suspended matter based calculated erosion rate. Therefore, the mobilization of silica and silicate cations seems to be decoupled during the monsoon season to some extent.

However, most dissolved fluxes stem from carbonate weathering and the long-term effect of erosion on weathering fluxes is due the sedimentation of reactive material in the lower reaches of the basin.

5.7. Runoff control

Intense precipitation during the monsoon season controls discharge (Fig. 6) and the chemical composition and fluxes of measured parameters via runoff (Figures S3-S4 and Figs. 7–10). Precipitation enhances physical erosion rates and supply sediments to the fluvial networks and the lower reaches (Bookhagen, 2010; Roback et al., 2018). These results suggest that precipitation patterns and runoff, in combination, represents a dominant regulator of weathering rates within the central Himalaya for the recent time scale (Fig. 12d, e). Similar results were reported earlier from the same region (France-Lanord et al., 2003; Tipper et al., 2006; Gabet et al., 2008; Bickle et al., 2018) and from other basins of the world (White and Blum, 1995; Gaillardet et al., 1999).

5.8. Comparison of weathering rates with largest rivers of the world

Annual dissolved silica and cationic export rate, and runoff from Q1 and Q2, are relatively high when compared with the world's large rivers (Table 6, Fig. 12d, e), while data for Q3 are relatively close to world average values.

Table 6
Comparison of the cationic and silica flux rate of the Langtang Narayani basin with large river basins of the world sorted by runoff. World average data from Livingston (1963); Brahmaputra, Ganga, Indus, and Yamuna data from Sarin et al. (1989); and other major river data from Meybeck and Ragu (1997) and Gaillardet et al. (1999).

River Basins	Runoff m yr^{-1}	SiO_2 Export Rate tons km^{-2} yr^{-1}	Cationic Export Rate tons km^{-2} yr^{-1}	River Basins	Runoff m yr^{-1}	SiO_2 Export rate tons km^{-2} yr^{-1}	Cationic Export Rate tons km^{-2} yr^{-1}
Kikori	3.03	24.25	130.22	**World Average**	**0.31**	**3.87**	**8.04**
Purari	2.75	37.99	75.48	Rhine	0.31	1.62	58.70
Fly	2.31	20.83	59.78	Panuco	0.26	nd	45.4
Sepik	1.52	19.06	35.7	Danube	0.25	1.05	26.65
Narayani (this study)	**1.45**	**12.72**	**78.56**	Indus	0.25	1.25	10.56
Trishuli (this study)	**1.27**	**9.96**	**35.70**	Yenissei	0.24	1.98	6.33
Irrawady	1.19	11.89	56.9	Cauveri	0.24	4.55	28.05
Amazon	1.08	7.45	9.67	Yukon	0.24	1.81	10.09
Brahmaputra	1.05	8.20	22.97	Khatanga	0.23	0.75	6.29
Orinoco	1.03	6.51	5.57	Weser	0.23	0.93	190
Hong He	1.03	10.28	37.14	Lena	0.21	1.23	5.79
Magdalena	1.01	12.73	28.79	Ebro	0.21	2.20	34.9
Xijiang	0.83	7.09	34.20	Parana	0.20	3.49	3.68
Po	0.67	2.69	62.7	Kolima	0.20	0.81	3.57
Yamuna	0.66	6.83	35.00	Nemanus	0.20	0.41	21.73
Salween	0.65	nd	47.5	Mississippi	0.19	1.49	11.05
Uruguay	0.60	9.08	7.57	Amur	0.19	0.40	2.81
Langtang (this study)	**0.6**	**2.95**	**9.85**	Mackenzie	0.17	0.52	9.04
Mekong	0.59	5.89	38.86	Wisla	0.16	nd	27.9
Rhone	0.56	2.27	51.3	Seine	0.16	1.05	23.07
Changjiang	0.51	3.33	27.00	Odra	0.16	nd	27.9
Fraser	0.51	2.78	12.7	Elbe	0.15	0.62	36.2
Mahanadi	0.50	4.51	15.80	Ob	0.14	0.35	4.06
Tocantins	0.49	5.70	3.56	Niger	0.13	1.80	1.32
Kuskokwin	0.49	3.72	15.94	Krishna	0.12	0.58	10.03
Pechora	0.40	0.66	6.96	Dnepr	0.11	0.37	7.46
Ganga	0.40	3.32	18.19	Shatt el arab	0.08	0.58	9.15
Narmada	0.38	3.45	30.30	Nelson	0.08	0.11	4.92
Columbia	0.35	3.18	10.27	Zambese	0.08	1.30	1.71
Godavari	0.34	7.09	14.41	Don	0.07	0.02	18.3
St. Lawrence	0.33	0.79	14.18	Limpopo	0.06	1.05	3.36
Congo-Zaire	0.32	3.06	2.46	Huanghe	0.05	0.42	6.89
N. Dvina	0.32	0.72	13.7	Nile	0.03	0.37	3.03
				Murray Darling	0.02	0.11	3.23

The dissolved silica export rate resulted comparable with that documented by France-Lanord et al. (2003) in the same region (except some catchments within the Annapurna basin, which have much higher export rates, up to 105 tons km^{-2} yr^{-1}). The Ganga-Brahmaputra Himalayan river system ranks first in terms of sediment transport to the ocean on a global scale (Milliman and Meade, 1983; Sarin et al., 1989). Milliman and Syvitski (1992) reported about 20 billion tons of sediment transported by rivers annually to the world oceans before the construction of dams in the latter half of this century. As shown in Table 5 we calculated 1,611 tons km^{-2} yr^{-1} from the Narayani at Q1, which yields 51.2 million tons per year from our study area. This sediment transport rate is slightly higher than for other mountain river systems in the region such as Narmada (1,400 tons km^{-2} yr^{-1}) and Damodar (1,400 tons km^{-2} yr^{-1}) in India. Moreover, the export rate at Q1 is significantly higher than for the larger Himalayan river systems such as the Brahmaputra (890 tons km^{-2} yr^{-1}) and the Ganga (530 tons km^{-2} yr^{-1}) as reported by Subramanian and Ittekkot (1991) and Milliman and Syvitski (1992), and is 10.7 times higher than the world average rate (Milliman and Meade, 1983).

6. CONCLUSIONS

Spatiotemporal variability of controlling factors on major solutes was studied for the Langtang-Narayani river system. For this purpose, trends with elevation and the influence of seasonality on the annual export rates were evaluated. Lower elevations showed higher weathering rates while at the same time the system is fed by new sediments from the higher elevations. Carbonate weathering is dominant, and the potential amount of sulfide oxidation may equal idealized silicate CO_2-consumption.

During the monsoon season (the period responsible for the export of most of the matter) no clear dilution effect lasting the whole season for the most important weathering products, alkalinity, $^{*}SO_4$, $^{*}Ca$ and $^{*}Mg$, was identified for the lowest sampling sites. Rather, we observed a pulse like

increase in concentrations during the middle of the monsoon season. This suggests that the monsoon season accelerates the mobilization of the dominant weathering products in the lower reaches, the location with the highest weathering rates. Therefore, it will be interesting to study how seasonality patterns and their variability affect long-term weathering fluxes. Specifically, to consider climate change and processes such as landslide mobilization, soil-rock water mobilization as a pulse-like mobilization during wet seasons or areas of pyrite oxidation and mobilization of their products.

ACKNOWLEDGEMENTS

M.B. and J.H. thank Tom Jäppinen, Thorben Amann, Andreas Weiss, and Lisett Kretzschmann for their help in the laboratory. The authors are grateful to Kedar Rijal, Anil Shrestha and Bijaya Pokhrel for their help and cooperation for the preparation of fieldwork. Thanks to Quinga Tamang, Mingma Tamang, Deepak Bhatt, Rajan Subedi, Gyanendra Pant, Gyan Shrestha, Bibek Karki, Sushil Karki, Suraj Poudyal and other members of the field campaign for their help and cooperation during the sampling. The authors gratefully acknowledged to the Department of Hydrology and Meteorology (DHM), Government of Nepal for providing hydrology data. This research was supported by the German Science Foundation DFG through the Cluster of Excellence 'CliSAP' (EXC177), Universität Hamburg. M.B. thanks Ronny Lauerwald for calculation of inorganic carbon species by using the PhreeqC model. The authors thank two anonymous reviewers for detailed, constructive comments and the associate editor Anthony Dosseto for suggestions that helped to improve the manuscript.

APPENDIX A. SUPPLEMENTARY MATERIAL

Supplementary data associated with this article can be found, in the online version, at https://doi.org/10.1016/j.gca.2018.06.033.

REFERENCES

Abril G., Bouillon S., Darchambeau F., Teodoru C. R., Marwick T. R., Tamooh F., Ochieng Omengo F., Geeraert N., Deirmendjian L., Polsenaere P. and Borges A. V. (2015) Technical note: large overestimation of pCO_2 calculated from pH and alkalinity in acidic, organic-rich freshwaters. *Biogeosciences* **12**, 67–78.

Acevedo M. F. (2013) *Data Analysis and Statistics for Geography, Environmental Science and Engineering. Applications to Sustainability. Boca Raton*. CRC Press, Taylor and Francis Group, Florida, p. 535.

Aitkenhead J. A. and McDowell W. H. (2000) Soil C:N ratio as a predictor of annual riverine DOC flux at local and global scales. *Global Biogeochem. Cycles* **14**(1), 127–138.

Andermann C., Longuevergne L., Bonnet S., Crave A., Davy P. and Gloaguen R. (2012) Impact of transient groundwater storage on the discharge of Himalayan rivers. *Nature Geosci.* **5**, 127–132.

Anderson S. P., Blum J., Arbor A., Brantley S. L., Chawdick O., Derry L. A., Drever J. I., Hering J. G., Kirchner J. W., Kump L. R., Richter D. and White A. F. (2004) Proposed initiative would study earth's weathering engine. *EOS Trans., AGU* **85** (28), 265–269.

Barnard P. L., Owen L. A., Finkel R. C. and Asahi K. (2006) Landscape response to deglaciation in a high relief, monsoon-influenced alpine environment, Langtang Himal, Nepal. *Quaternary Sci. Rev.* **25**(17–18), 2162–2176.

Bhatt M. P. and McDowell W. H. (2007) Controls on major solutes within the drainage network of a rapidly weathering tropical watershed. *Water Resour. Res.* **43**, W11402. https://doi.org/10.1029/2007WR005915.

Bhatt M. P., Takeuchi N. and Acevedo M. F. (2016) Chemistry of supraglacial ponds in the debris covered area of Lirung glacier in central Nepal Himalayas. *Aquatic Geochem.* **22**(1), 35–64. https://doi.org/10.1007/s10498-015-9276-9.

Bhatt M. P., Masuzawa T., Yamamoto M. and Takeuchi N. (2007) Chemical characteristics of pond waters within the debris area of Lirung Glacier in Nepal Himalaya. *J. Limnol.* **66**(2), 71–80.

Bhatt, M.P., Masuzawa, T., Yamamoto, M., McDowell, W.H., 2008. Chemical weathering in central Himalaya: Dissolved silica dynamics in glacier meltwater. In: International Conference on Hydrology and Climate Change in Mountainous Area (ICHCC), SOHAM – UNESCO, Kathmandu, pp. 162–179.

Bhatt M. P., Masuzawa T., Yamamoto M. and Gardner K. H. (2009) Spatial variations in chemical compositions along Langtang-Narayani river system in central Nepal. *Environ. Geol.* **57**, 557–569. https://doi.org/10.1007/s00254-008-1325-x.

Bhatt, M.P., Masuzawa, T., Yamamoto, M., Sakai, A., Fujita, K., 2000. Seasonal changes in dissolved chemical composition and flux of melt water draining from Lirung glacier in the Nepal Himalayas. In: Proceedings of a workshop on Debris-Coved Glaciers held at Seattle, Washington, USA. IAHS Publ. no. 264, pp. 277–288.

Bickle M. J., Chapman H. J., Tipper E., Galy A., De La Rocha C. L. and Ahmad T. (2018) Chemical weathering outputs from the floodplain of the Ganga. *Geochim. Cosmochim. Acta* **225**, 146–175.

Bookhagen B. (2010) Appearance of extreme monsoonal rainfall events and their impact on erosion in the Himalaya. *Geomatics, Nat. Hazards Risk* **1**(1), 37–50.

Börker J., Hartmann J., Romero-Mujalli G. and Li G. (2018) Short Communication: aging of basalt volcanic systems and decreasing CO_2 consumption by weathering. *Earth Surf. Dynam. Discuss.*. https://doi.org/10.5194/esurf-2018-10.

Brouand, M., 1989. Petrogenese des migmatite de la dalle du Tibet (Himalaya du Nepal). PhD thesis, INPL, Nancy, France.

Calmels D., Gaillardet J., Brenot A. and France-Lanord C. (2007) Sustained sulfide oxidation by physical erosion processes in the Mackenzie River basin: climatic perspectives. *Geology* **35**, 1003.

Chaudhary R. P., Upreti Y. and Rimal S. K. (2016) Deforestation in Nepal: Causes, Consequences and Responses. In *Biological and Environmental Hazards, Risks, and Disasters* (eds. J. F. Shroder and R. Sivanpillari). Elsevier Inc., pp. 335–372.

Collins R. and Jenkins A. (1996) The impact of agricultural land use on stream chemistry in the middle hills of the Himalayas, Nepal. *J. Hydrol.* **185**(1–4), 71–86.

CRAN, 2018. The Comprehensive R Archive Network. Accessed February 2018. Available from: <https://cran.r-project.org/>

Dalai T. K., Krishnaswami S. and Sarin M. M. (2002) Major ion chemistry in the headwaters of the Yamuna river system: chemical weathering, its temperature dependence and CO_2 consumption in the Himalaya. *Geochim. Cosmochim. Acta* **66** (19), 3397–3416.

Degens E. T., Kempe S. and Richey J. E. (1991). In *Biogeochemistry of Major World Rivers*. Wiley, New York, pp. 1–356.

Dessert C., Dupre B., Gaillardet J., Francois L. and Allegre C. (2003) Basalt weathering rate laws and the impacts of basalt weathering on the global carbon cycle. *Chem. Geol.* **202**, 257–273.

DHM, Department of Hydrology and Meteorology, 2008. Hydro-meteorological data of Nepal, DHM, Government of Nepal, Kathmandu.

DMG, Department of Mines and Geology, 1980. Geological Map of Central Nepal. Department of Mines and Geology, His Majesty's Government of Nepal, Kathmandu, Nepal.

DMG, Department of Mines and Geology, 1994. Geological Map of Nepal. Department of Mines and Geology, His Majesty's Government of Nepal, Kathmandu, Nepal.

Drever J. I. (1988) *The Geochemistry of Natural Waters*, second ed. Prentice Hall, Englewood Cliffs, p. 473.

Edmond J. M. and Huh Y. (1997) Chemical weathering yields from basement and orogenic terrains in hot and cold climates. In *Tectonic Uplift and Climate Change* (ed. W. F. Ruddiman). Plenum Press, pp. 329–351.

Evans M. J., Derry L. A. and France-Lanord C. (2008) Degassing of metamorphic carbon dioxide from the Nepal Himalaya. *Geochem. Geophys. Geosyst.* **9**(4), Q04021. https://doi.org/10.1029/2007GC001796.

France-Lanord C. and Derry L. A. (1997) Organic carbon burial forcing of the carbon cycle from Himalayan erosion. *Nature* **390**, 65–67.

France-Lanord C., Evans M., Hurtrez J. E. and Riotte J. (2003) Annual dissolved fluxes from central Nepal rivers: budget of chemical erosion in the Himalayas. *Comptes Rendus Geosci.* **335** (16), 1131–1140.

Gabet E. J., Burbank D. W., Putkonen J. K., Pratt-Sitaula B. A. and Ojha T. (2004) Rainfall thresholds for landsliding in the Himalayas of Nepal. *Geomorphology* **63**(3–4), 131–143.

Gabet E. J., Burbank D. W., Pratt-Sitaula B., Putkonen J. and Bookhagen B. (2008) Modern erosion rates in the High Himalayas of Nepal. *Earth Planet. Sci. Lett.* **267**, 482–494.

Gaillardet J., Dupre B., Louvat P. and Allegre C. J. (1999) Global silicate weathering and CO_2 consumption rates deduced from the chemistry of large rivers. *Chem. Geol.* **159**(17), 3–30.

Galy A. and France-Lanord C. (1999) Weathering processes in the Ganga-Brahmaputra basin and the riverine alkalinity budget. *Chem. Geol.* **159**(1–4), 31–60.

Gansser A. (1964) *Geology of the Himalayas*. Intersciences Publisher, LU.

Garrels, R.M., Mackenzie, F.T., 1967. Origin of the chemical compositions of some springs and lakes. In: Equilibrium Concepts in Natural Water System, Advanced Chemistry Series 67. Am. Chem. Soc., Washington DC, pp. 222–242.

Garrels R. M. and Mackenzie F. T. (1971) *Evolution of Sedimentary Rocks*. W. W Norton and Company Inc., New York, p. 397.

Goldschmidt S. T., Lyons W. B., Harmon R. S., Harmon B. A., Carey A. E. and McElwee G. T. (2015) Organic carbon concentrations and transport in small mountain rivers, Panama. *Appl. Geochem.* **63**, 540–549.

Hartmann J., Lauerwald R. and Moosdorf N. (2014) A brief overview of the global river chemistry database, GLORICH. *Proc. Earth Planet. Sci.* **10**, 23–27.

Hartmann J., Jansen N., Kempe S. and Dürr H. H. (2007) Geochemistry of the river Rhine and the upper Danube: recent trends and lithological influence on base lines. *J. Environ. Sci. Sustain. Soc.* **1**(39), 39–46.

Hasnain S. I. and Thayyen R. J. (1999) Controls on the major ion chemistry of Dokriani glacier meltwaters, Ganga basin, Garhwal Himalaya, India. *J. Glaciol.* **45**, 87–92.

Hu M. H., Stallard R. F. and Edmond J. M. (1982) Major ion chemistry of some large Chinese rivers. *Nature* **298**, 550–553.

Ibarra D. E., Caves J. K., Moon S., Thomas D. L., Hartmann J., Chamberlain C. P. and Maher K. (2016) Differential weathering of basaltic and granitic catchments from concentration-discharge relationship. *Geochim. Cosmochim. Acta* **190**, 265–293.

Inger S. and Harris B. W. (1992) Tectonothermal evolution of the high Himalayan crystalline sequence, Langtang valley, Northern Nepal. *J. Metam. Geol.* **10**, 439–452.

Jin Z., West A. J., Zhang F., An Z., Hilton R. G., Yu J., Wang J., Li G., Deng L. and Wang X. (2016) Seismically enhanced solute fluxes in the Yangtze River headwaters following the A.D. 2008 Wenchuan earthquake. *Geology* **44**(1), 47–50. https://doi.org/10.1130/G37246.1.

Kansakar S. R., Hannah D. M., Gerrard J. and Rees G. (2004) Spatial pattern in the precipitation regime of Nepal. *Int. J. Climatol.* **24**, 1645–1659.

Keene W. C., Pszenny A. A. P., Galloway J. N. and Hawley M. E. (1986) Sea-salt corrections and interpretation of constituent ratios in marine precipitation. *J. Geophys. Res.* **91**(No.D6), 6647–6658.

Kempe, S., 1982. Long-term records of CO_2 pressure fluctuations in fresh water. In: Degens, E.T., (Ed.), Transport of Carbon and Minerals in Major World Rivers Part 1, pp. 91–332.

Lauerwald R., Hartmann J., Ludwig W. and Moosdorf N. (2012) Assessing the nonconservative fluvial fluxes of dissolved organic carbon in North America. *J. Geophys. Res.* **117**, G01027. https://doi.org/10.1029/2011JG001820.

Lauerwald R., Laruelle G. G., Hartmann J., Ciais P. and Regnier P. A. G. (2015) Spatial patterns in CO_2 evasion from the global river network. *Global Biogeochem. Cycles* **29**, 534–554. https://doi.org/10.1002/2014GB004941.

Livingston, D.A., 1963. Chemical compositions of rivers and lakes. USGS professional paper 400-G, G1-G64.

Lupker M., France-Lanord C., Galy V., Lave J., Gaillardet J., Gajurel A. P., Guilmette C., Rahman M., Singh S. K. and Sinha R. (2012) Predominant floodplain over mountain weathering of Himalayan sediment (Ganga basin). *Geochim. Cosmochim. Acta* **84**, 410–432.

Maher K. and Chamberlain C. P. (2014) Hydrologic regulation of chemical weathering and the geologic carbon cycle. *Science* **343**, 1502–1504.

McDowell W. H., Sanchez C. G., Asbury C. E. and Ramos Perez C. R. (1990) Influence of sea salt aerosols and long range transport on precipitation chemistry at El Verde, Puerto Rico. *Atmos. Environ.* **24**(11), 2813–2821.

Meybeck M. (1982) Carbon, nitrogen, and phosphorus transport by world rivers. *Am. J. Sci.* **282**, 401–450.

Meybeck M. (1987) Global chemical weathering from surficial rocks estimated from river-dissolved loads. *Am. J. Sci.* **287**, 401–428.

Meybeck M. and Ragu A. (1997) *River Discharges to the Oceans: An Assessment of Suspended Solids, Major Ions and Nutrients. UNEP/WHO, Environment of Information and Assessment Division*. UNEP, Nairobi, p. 245.

Milliman J. D. and Meade R. H. (1983) World-wide delivery of river sediments to the Oceans. *J. Geol.* **91**, 1–21. https://doi.org/10.1086/628741.

Milliman J. D. and Syvitski J. P. M. (1992) Geomorphic tectonic control of sediment discharge to the ocean – the importance of small mountainous rivers. *J. Geol.* **100**(5), 525–544.

Millot R., Gaillardet J., Dupre B. and Allegre C. J. (2002) The global control of silicate weathering rates and the coupling with physical erosion: new insights from rivers of the Canadian Shield. *Earth Planet. Sci. Lett.* **196**, 83–98.

Millot R., Gaillardet J., Dupre B. and Allegre C. J. (2003) Northern latitude chemical weathering rates: clues from the Mackenzie River Basin, Canada. *Geochim. Cosmochim. Acta* **67** (7), 1305–1329.

Navarre-Sitchler A. and Brantley S. L. (2007) Basalt weathering across scales. *Earth Planet. Sci. Lett.* **261**, 321–334.

Ohta T., Fukushima Y., Suzuki M., Motoyama H., Kawashima K. and Kubota H. (1987) Suspended sediment yield in a glaciated watershed of Langtang valley, Nepal Himalayas. *Jap. Soc. Snow Ice Bull. Glacier Res.* **5**, 19–24.

Oliva P., Viers J. and Dupré B. (2003) Chemical weathering in granitic environments. *Chem. Geol.* **202**(3–4), 225–256.

Parkhurst, D.I., Appelo, C.A.I., 1999. User's guide to PHREEQC: A computer program for speciation, reaction path, 1D transport and inverse geochemical calculations. US Geological Survey, Water Resources Investigations Report 99-4259.

Raymo M. E. and Ruddiman W. F. (1992) Tectonic forcing of late Cenozoic climate. *Nature* **359**, 117–122.

Raymond P. A., Hartmann J., Lauerwald R., Sobek S., McDonald C., Hoover M., Butman D., Striegl R., Mayorga E., Humborg C., Kortelainen P., Dürr H., Meybeck M., Ciais P. and Guth P. (2013) Global carbon dioxide emissions from inland waters. *Nature* **503**(7476), 355–359.

Roback K., Clark M. K., West A. J., Zekkos D., Li G., Gallen S. F., Chamlagain D. and Godt J. W. (2018) The size, distribution, and mobility of landslides caused by the 2015 Mw 7.8 Gorkha earthquake, Nepal. *Geomorphology* **301**, 121–138.

Roth J. (1878) *Flusswasser, Meerwasser, Steinsalz*. Verlag von Carl Habel, Berlin.

Roth J. (1879) *Allgemeine und Chemische Geologie, Erster Band—Bildung und Umbildung der Mineralien. Quell-, Fluss- und Meerwasser. Die Absätze*. Verlag von Wilhelm Hertz (Bessersche Buchhandlung), Berlin.

Roth J. (1893) *Allgemeine und Chemische Geologie, Dritter Band—Zweite Abteilung: Verwitterung, Zersetzung und Zerstörung der Gesteine*. Verlag von Wilhelm Hertz (Bessersche Buchhandlung), Berlin.

Sarin M. M., Krishnaswami S., Dilli K., Somayajulu B. L. K. and Moore W. S. (1989) Major ion chemistry of the Ganga-Brahmaputra river system: weathering processes and fluxes to the Bay of Bengal. *Geochim. Cosmochim. Acta* **53**, 997–1009.

SD, 1983. Physiographic Regions of Nepal. Topographical Survey Branch, Survey Department. Ministry of Land Reform, HMG, Kathmandu, Nepal.

SD, 1984. Land System Map, Central Development Region, Nepal. Topographical Survey Branch, Survey Department. Ministry of Land Reform, HMG, Kathmandu, Nepal.

Singh S. K., Sarin M. M. and France-Lanord C. (2005) Chemical erosion in eastern Himalaya: Major ion composition of the Brahmaputra and $\delta^{13}C$ of dissolved inorganic carbon. *Geochim. Cosmochim. Acta* **69**(14), 3573–3588.

Smithson S. B. (1971) Densities of metamorphic rocks. *Geophysics* **36**(4), 690–694.

Stainton J. D. A. (1972) *Forests of Nepal*. John Murray, London, p. 181.

Stallard R. F. (2000) Tectonic processes and erosion. *Int. Geophys.* **72**, 195–229.

Stallard R. F. and Edmond J. M. (1983) Geochemistry of the Amazon 2. The influence of geology and weathering environment on the dissolved load. *J. Geophys. Res.* **88**(C14), 9671–9688.

Struyf E. and Conley D. J. (2011) Emerging understanding of the ecosystem silica filter. *Biogeochemistry* **107**(1–3), 9–18.

Subramanian V. and Ittekkot V. (1991) Carbon transport in Himalayan rivers. In *SCOPE 42: Biogeochemistry of Major World Rivers* (eds. D. Eisma and S. Kempe). Wiley and Sons, England, pp. 159–170.

Tipper E. T., Bickle M. J., Galy A., West A. J., Pomies C. and Chapman H. J. (2006) The short term climatic sensitivity of carbonate and silicate weathering fluxes: insight from seasonal variations in river chemistry. *Geochim. Cosmochim. Acta* **70**(11), 2737–2754.

Torres M. A., West A. J. and Li G. (2014) Sulphide oxidation and carbonate dissolution as a source of CO_2 over geologic timescales. *Nature* **507**, 346–349.

Torres M. A., Moosdorf N., Hartmann J., Adkins J. F. and West A. J. (2017) Glacial weathering, sulfide oxidation, and global carbon cycle feedbacks. *Proc. Natl. Acad. Sci. USA* **114**(33), 8716–8721.

Torres M. A., West A. J., Clark K. E., Paris G., Bouchez J., Ponton C., Feakins S. J., Galy V. and Adkins J. F. (2016) The acid and alkalinity budgets of weathering in the Andes-Amazon system: insights into the erosional control of global biogeochemical cycles. *Earth Planet. Sci. Lett.* **450**, 381–391.

Tranter M. and Raiswell R. (1991) The composition of the englacial and subglacial component in bulk meltwaters draining the Gornergletscher, Switzerland. *J. Glaciol.* **37**, 59–66.

Tranter M., Brown G., Raiswell R., Sharp M. and Gurnell A. (1993) A conceptual model of solute acquisition by Alpine glacier meltwaters. *J. Glaciol.* **39**, 573–581.

West A. J., Galy A. and Bickle M. (2005) Tectonic and climate controls on silicate weathering. *Earth Planet. Sci. Lett.* **235**(1–2), 211–228.

White A. F. and Blum A. E. (1995) Effects of climate on chemical weathering in watersheds. *Geochim. Cosmochim. Acta* **59**(9), 1729–1747.

Wolff-Boenisch W., Gabet E., Burbank D. W., Langner H. and Putkonen J. (2009) Spatial variations in chemical weathering and CO_2 consumption in Nepalese High Himalayan catchments during monsoon season. *Geochim. Cosmochim. Acta* **73**, 3148–3170.

WWF-Nepal, 2005. An overview of glaciers, glacier retreat, and subsequent impacts in Nepal, India, and China. Kathmandu, Nepal, p. 70.

Associate Editor: Anthony Dosseto